PERGAMON

Journal of Structural Geology 23 (2001) 1781–1802

JOURNAL OF STRUCTURAL GEOLOGY

www.elsevier.com/locate/jstrugeo

Dynamic recrystallization processes in plagioclase porphyroclasts

Robert Kruse[a], Holger Stünitz[a,*], Karsten Kunze[b]

[a]*Geologisches Institut, Universität Basel, Bernoullistr. 32, 4056 Basel, Switzerland*
[b]*Geologisches Institut, ETH-Zentrum, 8092 Zürich, Switzerland*

Received 11 August 2000; revised 8 February 2001; accepted 15 February 2001

Abstract

Recrystallization processes in plagioclase porpyroclasts were studied in samples from an anorthositic gabbro of the Jotun Complex, South Norwegian Caledonides. The deformation took place at a temperature of approximately 700°C and at pressures below 900 MPa. Two populations of plagioclase porphyroclasts can be distinguished based on microstructural observations. The crystallographic orientation and grain shapes for the two populations are interpreted as 'soft' and 'hard' orientations of the dominant slip system (010)[001] with respect to the kinematic reference system. The orientations of porphyroclasts and recrystallized grains were measured with a U-stage microscope. Analysis of misorientations between porphyroclasts and adjacent recrystallized grains yields different results for the two types of porphyroclasts. In type-1 porphyroclasts (soft orientation) the misorientation is inferred to be caused by subgrain rotation due to the activation of the (010)[001] slip system, resulting in a host control orientation relationship, whereas in type-2 porphyroclasts (hard orientation) no dominant misorientation relationship could be identified. The slip systems of the dislocations inferred from transmission electron microscopy (TEM) analysis correspond well with the results of the U-stage misorientation analysis. In type-2 porphyroclasts (hard orientation) micro-fracturing was observed in the TEM, whereas microfractures are absent in type-1 porphyroclasts (soft orientation). Micro-fracturing is likely to be the mechanism for nucleation of new grains in type-2 porphyroclasts, resulting in a no-host control orientation relationship between porphyroclasts and recrystallized grains.

Keywords: Plagioclase; Crystallographic preferred orientation (CPO); Misorientation; Dynamic recrystallization; Subgrain rotation; Micro-fracturing

1. Introduction

Dynamic recrystallization commonly takes place by two processes: grain boundary migration and progressive subgrain rotation (Poirier and Guillopé, 1979; Urai et al., 1986; Drury and Urai, 1990). One of the microstructural characteristics by which dominant recrystallization processes can be distinguished from each other is the crystallographic orientation of recrystallized grains with respect to the parent (host) grains. Progressive subgrain rotation typically results in a 'host control' of the recrystallized grains, whereas for migration-dominated recrystallization processes, the factors controlling the orientation of recrystalllized grains may be difficult to recognize (Drury and Urai, 1990; Ji and Mainprice, 1990; Dornbusch et al., 1994). If both recrystallization processes operate simultaneously, the dominant process can be identified by a misorientation analysis. The misorientation increases in the subgrain boundary with increasing dislocation density, until the subgrain boundary turns into a large angle grain boundary, whose orientation may be modified by subsequent grain boundary migration (Fitz Gerald et al., 1983; Cahn, 1983; Drury et al., 1985; Drury and Urai, 1990). Thus, the observed grain boundary geometry does not necessarily represent the initial relationship between neighboring grains. The crystallographic misorientation between two grains, however, is not changed by grain boundary migration and provides a useful tool for determining the recrystallization process.

During recrystallization, the crystallographic orientations of grains change and grains of certain orientations may grow while others are consumed. Growth, consumption, and the dominant recrystallization process depend strongly on dislocation densities and whether certain slip systems are activated. Activation of slip systems and dislocation densities depend on the orientation of the crystals with respect to the principal stress directions. Grains can be divided into populations having 'soft orientations' (crystals suitably oriented for slip; high resolved shear stresses on the slip systems) and 'hard orientations' (crystals unsuitably oriented for slip (Burg et al., 1986; Schmid, 1994); low resolved shear stresses). Karato (1987; 1988) showed that rates of recrystallization and re-orientation are different in grains of 'hard' and 'soft orientation'.

* Corresponding author. Tel.: +41-61-267-3596; fax: +41-61-267-3613.
E-mail address: holger.stuenitz@unibas.ch (H. Stünitz).

0191-8141/01/$ - see front matter
PII: S0191-8141(01)00030-X

The main objective of this study is the analysis of recrystallization processes and their dependence on the orientation of porphyroclasts within a mylonite. For example, are dominant recrystallization processes different for 'soft' and 'hard' orientations? Are there differences in the dislocation density for different crystal orientations?

We chose plagioclase as an example for such a study because the complete orientations of grains can be determined by light microscopy, and light microscopy allows a rapid quantitative analysis of other microstructural features, such as aspect ratios, twinning, etc. For plagioclase, migration-dominated recrystallization processes are most important in experimentally deformed samples (Tullis and Yund, 1985, 1987; Tullis et al., 1990) because of the limited climb of dislocations. Such migration microstructures correspond to regime 1 dislocation creep (low temperature plasticity) in quartz (Hirth and Tullis, 1992). In nature, rotation recrystallization is a very common dynamic recrystallization mechanism in plagioclase (Fitz Gerald et al., 1983; Jensen and Starkey, 1985; Olsen and Kohlstedt, 1985; Ji and Mainprice, 1990) but migration-related microstructures have been described, too (Goode, 1978; Olesen, 1987; Bell and Johnson, 1989; Ji and Mainprice, 1990; LaFrance et al., 1996). Consequently, the question arises: which recrystallization process is dominant, and which factors cause that dominance? Fracturing is another important process that affects the recrystallization of experimentally deformed plagioclase (Tullis and Yund, 1987, 1992; Tullis et al., 1990; McLaren and Pryer, 2001), and thus, it is one of the objectives of the present study to investigate the potential effect of fracturing on the recrystallization process in naturally deformed plagioclase.

2. Regional setting and sample description

Processes of dynamic recrystallization of plagioclase have been analyzed in mylonites from anorthosites of the Jotun nappe (South Norway), which were studied previously by Boullier and Gueguen (1975), Ji et al. (1988) and Ji and Mainprice (1988, 1990). The Jotun nappe forms a part of the Middle Allochthonous Unit of the Caledonides in southern Norway and consists of felsic and mafic intrusive and granulite facies metamorphic rocks that were subjected to a later regional metamorphism reaching amphibolite facies conditions at ca. 900 Ma (Schärer, 1980; Milnes and Koestler, 1985). During the late Scandian collision (ca. 420 Ma, Milnes et al., 1997) the Jotun nappe was thrusted about 300 km to the SE over the Baltic Shield (Hossack et al., 1985; Emmett, 1996; Milnes et al., 1997). During this thrusting event, deformation was restricted to a mylonite zone at the base of the Jotun nappe and took place under greenschist to lowermost amphibolite facies conditions. The largest part of the Jotun nappe remained unaffected by the thrusting (Milnes and Koestler, 1985) and consists of a large anorthositic gabbro intrusion, which is characterized by a granulite facies mineral assemblage of coarse-grained reddish plagioclase (An 48 – An 55) + orthopyroxene + clinopyroxene + brown hornblende + garnet. The layering consists of alternating bands of almost pure plagioclase and mafic minerals, which are centimeters to a decimeter thick (Fig. 1a). Primary magmatic olivine inclusions have developed corona structures with rims of orthopyroxene + clinopyroxene, and garnet + hornblende + spinel around olivine (Griffin, 1971; Griffin et al., 1985).

Locally, shear zones that predate the thrusting are present in the Jotun Nappe. They are centimeters to several meters thick, and in one locality form a 100-m-thick high strain zone, which is largely parallel to the base of the Jotun Complex but is never connected with the basal shear zone of the nappe (Kruse, 1998). The high strain zone was sampled in a quarry near the village of Eide, north of the road between Sogndal and Kaupanger, inner Sognefjord region (Topographical map 1:50.000, No. 1417 III, coordinates: 4015, 67876). The shear deformation is inhomogeneous and leads to the formation of protomylonites anastomosing around lenses of weakly deformed material. The foliation and lineation within the mylonites are defined by layers of recrystallized pyroxene and hornblende grains, which are used as reference orientations for the sample coordinate system. Higher shear strain is localized in thin (up to several centimeters) ultramylonites, in which the constituent phases are well mixed (Fig. 1b). The temperature and pressure conditions during this deformation have been estimated to be around 700°C at maximum pressures of ca. 900 MPa (Kruse and Stünitz, 1999).

3. Methods of study

Polished thin sections of three samples of different deformation intensity were cut parallel to the stretching lineation and perpendicular to the foliation. The same thin sections were used for U-stage measurements and microprobe analysis. Image analysis was applied to determine the proportions of recrystallized grains and porphyroclasts in the samples.

The crystallographic orientations of plagioclase porphyroclasts and adjacent recrystallized grains (usually 40–70 μm in diameter) were measured with a 4-circle U-stage. The crystallographic axes are not perpendicular to each other and not parallel to the axes of the optical indicatrix in triclinic plagioclase. The relationship between optical and crystallographic axes is a function of the anorthite content (Burri et al., 1967) and is determined as the angle between the indicatrix axes and at least one twin plane (albite or pericline twin) or cleavage plane [(010) or (001)]. Thus, the complete crystallographic orientation can be obtained by three independent measurements on a single plagioclase grain. The procedure for construction of the crystallographic axes according to Reinhard (1931), Burri et al. (1967), and Wenk et al. (1986) is supported by the computer program MIRACMS (Kruhl, 1987a) and

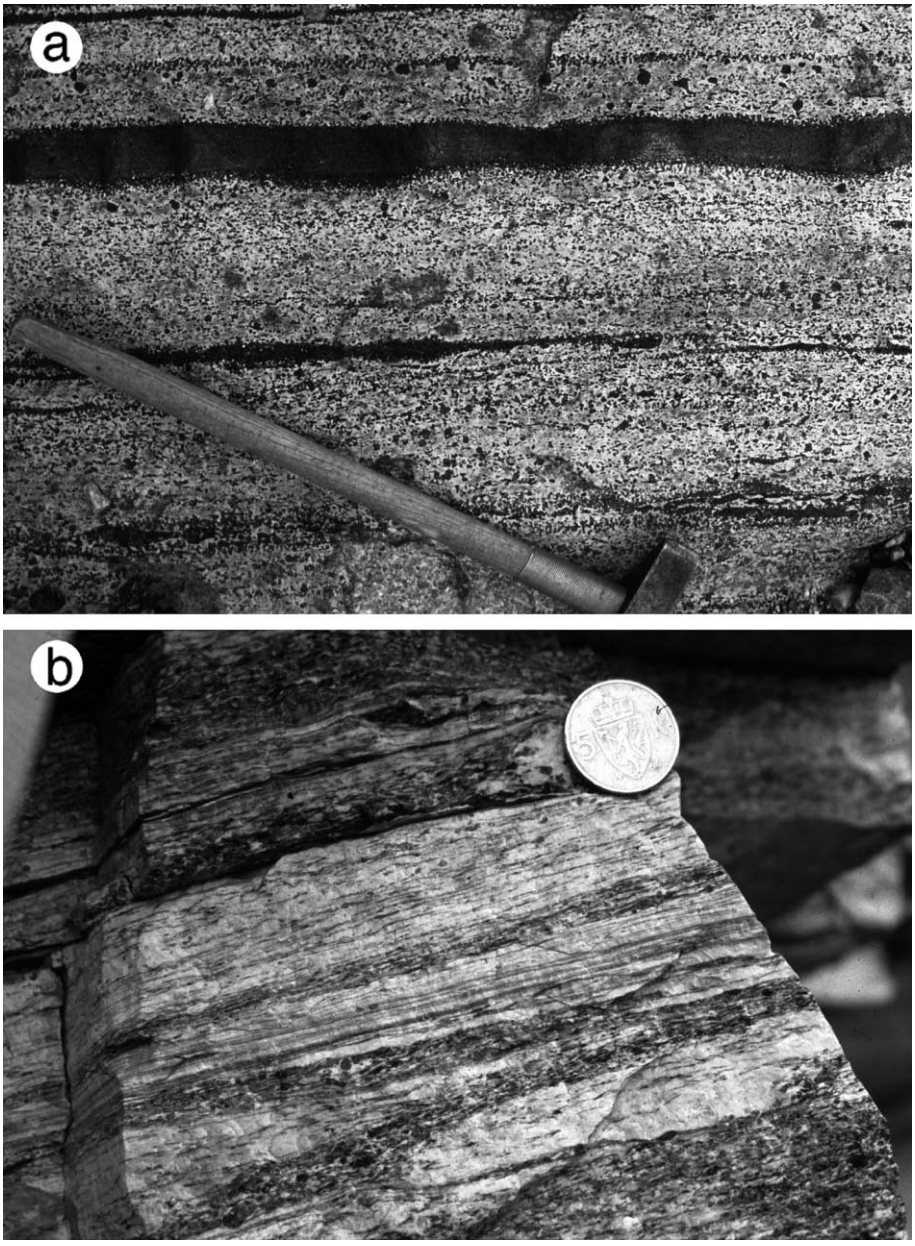

Fig. 1. (a) Undeformed anorthositic gabbro from the leucogabbro intrusion of the Jotun Complex (Middle Allochthonous unit) near Sogndal (Inner Sognefjord region, South Norway). (b) Mylonites forming a high strain zone within the anorthositic gabbro sub-parallel to the contact with the Lower Allochthonous Unit.

UNIPLAJ (Benn and Mainprice, 1989). An EXCEL spread sheet has been developed for the present study to calculate plagioclase orientations for the compositional range An 40–An 60 from measurements of indicatrix axes and twin or cleavage planes.

Chemical analyses were performed by WDX on a JEOL 8600 microprobe at 15 KV, 10 μA beam current, using natural standards and a PROZA correction routine. Ion-beam thinned foils were examined in a Hitachi H8000 TEM at 200 KV.

3.1. Misorientation analysis

The orientation relationship between porphyroclast and recrystallized grains is defined by the rotation of one crystal lattice onto the other, called misorientation (Randle, 1992, 1993), which is given by a rotation axis and a rotation angle (axis/angle pair). The rotation axis is a crystallographic direction common to both crystal lattices. It can be used to determine slip systems from features of intracrystalline deformation, like deformation bands, deformation lamellae, kink bands, or subgrains (olivine: Avé Lallemant, 1985; Toriumi and Karato, 1985; clinopyroxene: Buatier et al., 1991; quartz: Trépied et al., 1980; Mainprice et al., 1993; Fliervoet and White, 1995; Lloyd et al., 1997; plagioclase: Fitz Gerald et al., 1983). The misorientation axis/angle (m/θ) pair can either be constructed on a stereographic

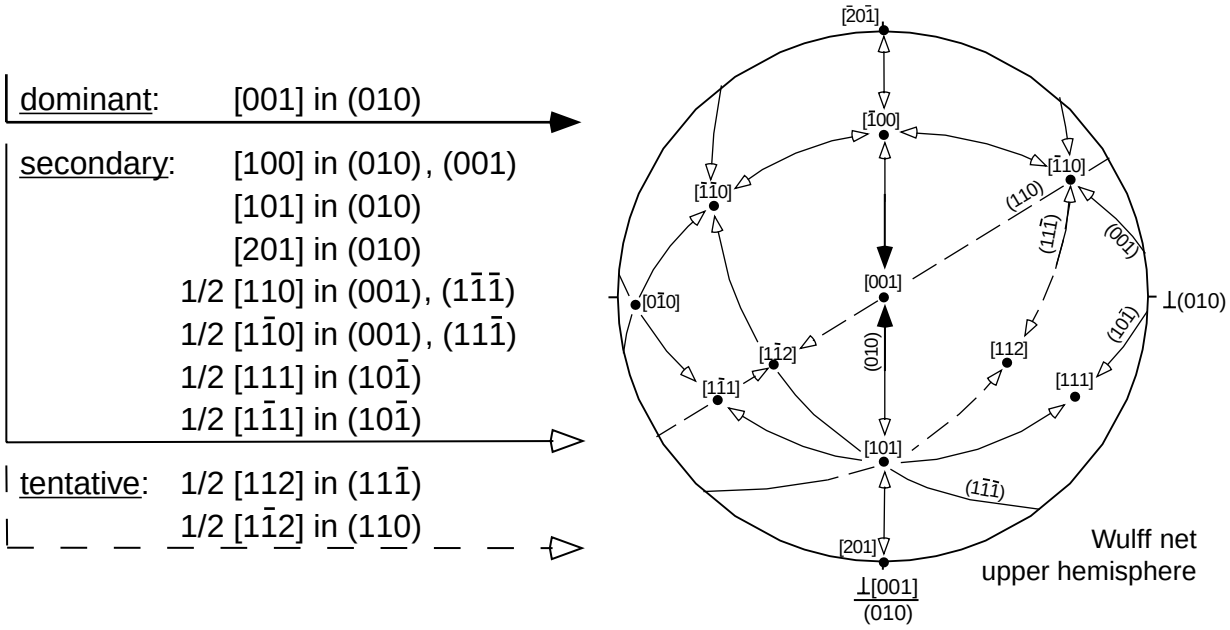

Fig. 2. Observed slip systems in intermediate plagioclase (C$\bar{1}$ space group) from TEM after Marshall and McLaren (1977) and Olsen and Kohlstedt (1984). The analysis of misorientation axes is based on the inverse pole figure as defined by Burri et al. (1967): pole to (010) to the east, [001] in the center, pointing upwards. The observed slip systems are presented in the pole figure as great circles (slip plane) and points (Burgers vector). The arrowheads indicate the slip plane, for which the Burgers vector is observed.

projection or calculated and is typically based on three non-coaxial crystallographic planes (hkl) and/or directions [uvw] of the measured grains (Randle, 1993, p. 102). The manual construction of the misorientation axes is described by Turner and Weiss (1963, p. 57) and Randle (1992, p. 135). In the present study the misorientation has been calculated according to the mathematical treatment of misorientation analysis given by Randle (1992, 1993) and Lloyd et al. (1997) and is summarized below.

After converting the spherical data (azimuth/dip) of three measurements [uvw], (hkl) of both porphyroclast and adjacent recrystallized grain to direction cosines, an orthogonal coordinate system is defined by a 3×3 matrix g_{ij}, which completely describes the orientation g of the crystal with respect to the sample reference coordinate system (Bunge, 1985). The rotation that transforms the orientation g of the grain into the reference coordinate system (identity matrix E) is given by the transverse matrix $g_{ij}^{\mathrm{T}} = g_{ji}$. Applying this rotation, which is defined by the orientation g_H of the reference grain (in this case the porphyroclast, host grain) to both, reference grain and recrystallized grain (orientation g_R), the reference grain will be transformed to the identity matrix E and the recrystallized grain will have an orientation different from E if its original orientation was different from the porphyroclast ($g_H \neq g_R$). The misorientation Δg between the two grains is given by the orientation of the recrystallized grain transformed by g_H^{T} and will be named misorientation matrix M_{ij} ($= g_R \times g_H^{\mathrm{T}}$) (i.e. Randle, 1992, 1993; Lloyd et al., 1997). From the misorientation matrix M_{ij} the misorientation axis/angle (m/θ) can be calculated (Kunze, 1991; Lloyd et al., 1997; Kruse, 1998). The misorientation axis is typically displayed in an inverse pole figure using the crystal reference frame (Bunge, 1985) but can also be transformed into the sample reference coordinate system. By convention, the crystal reference setting for an inverse pole figure of plagioclase is defined by $+(010)$ pole pointing to the east and $+[001]$ pointing upwards (Burri et al., 1967).

Since all plagioclase grains are strongly twinned it is often impossible to decide which is the original host orientation and which is the twin. The recrystallized grain may also have recrystallized from a twin of the host grain. The same problems arise if the recrystallized grain is twinned. Therefore, the measured misorientation is a superposition of the initial misorientation and a misorientation caused by twinning. Three types of twins are commonly found in these porphyroclasts: albite, pericline, and karlsbad twins; all have been considered in the misorientation analysis. All possible misorientation axis/angle pairs between a twinned porphyroclast and a twinned recrystallized grain provide physically correct solutions but the one with the least misorientation angle has been considered to represent the most reasonable misorientation relationship between two grains (Randle, 1992; Mainprice et al., 1993; Fliervoet, 1995; Lloyd et al., 1997).

3.2. Error estimation

The uncertainties of misorientation measurements depend on the misorientation angle and the measurement

accuracy of the applied technique to obtain the (hkl) and [uvw] (Fitz Gerald et al., 1983). A graphical solution to quantify the error of the determination of a rotation axis between two directions on the pole figure is given in Appendix A (Fig. A1). The maximum error of a misorientation axis between two crystallographic orientations may be calculated in an analogous way (Appendix A).

It can be seen that large errors have to be expected for small misorientation angles (below 10°) if the measurement accuracy is worse than 1°. The accuracy of the U-stage measurement is on the order of 2–3° (Siegesmund et al., 1994) and propagates to possible deviations of 24–37° at a misorientation angle of 10°. The equation given in Appendix A can be used to calculate the precision of a given method, which is necessary to achieve a desired accuracy of the misorientation between two orientations. Using the data of Prior (1999), the accuracy of absolute orientation measurements with the EBSD technique is about 0.8° (Fig. A2).

3.3. Identification of slip systems by misorientation analysis

The misorientation axes are given in pole figures with reference to the kinematic framework (x = parallel to the lineation, y = normal to the lineation within the foliation, z = perpendicular to the foliation). Inverse pole figures of the rotation axes have been calculated to obtain the crystallographic orientation of the misorientation axes with respect to the plagioclase host. The stereogram as defined by Burri et al. (1967) has been modified to display the slip systems of plagioclase. The known slip systems of intermediate plagioclase (C-1 space group) have been compiled from the literature and plotted in a stereographic projection (Fig. 2). Great circles indicate the slip planes and arrows indicate the Burgers vectors identified for a given slip plane.

The misorientation axes in such stereograms may be used to distinguish between misorientations due to an array of edge dislocations (tilt boundaries) or due to an array of screw dislocations (twist boundaries). The relationship between the misorientation axis and the slip system is given by the crystal structure and the type of dislocations accumulated in the (sub-) grain boundaries (Trépied et al., 1980; Mainprice et al., 1993; Lloyd et al., 1997). The misorientation axis has to lie within the slip plane for an array of edge dislocations (tilt-type misorientation, Fig. 3a) and perpendicular to it for an array of screw dislocations (twist-type misorientation, Fig. 3b) (Trépied et al., 1980; Poirier, 1985, p. 63). For orthorhombic or higher crystal symmetries the Burgers vector of edge dislocations is perpendicular to the misorientation axis (Lloyd et al., 1997), but this does not necessarily apply to triclinic plagioclase. For example, [100] in plagioclase is the orientation of the dislocation line of the "edge" segment of the (010)[001] slip system and will be the orientation of the corresponding misorientation axis. Since the angle between [100] and

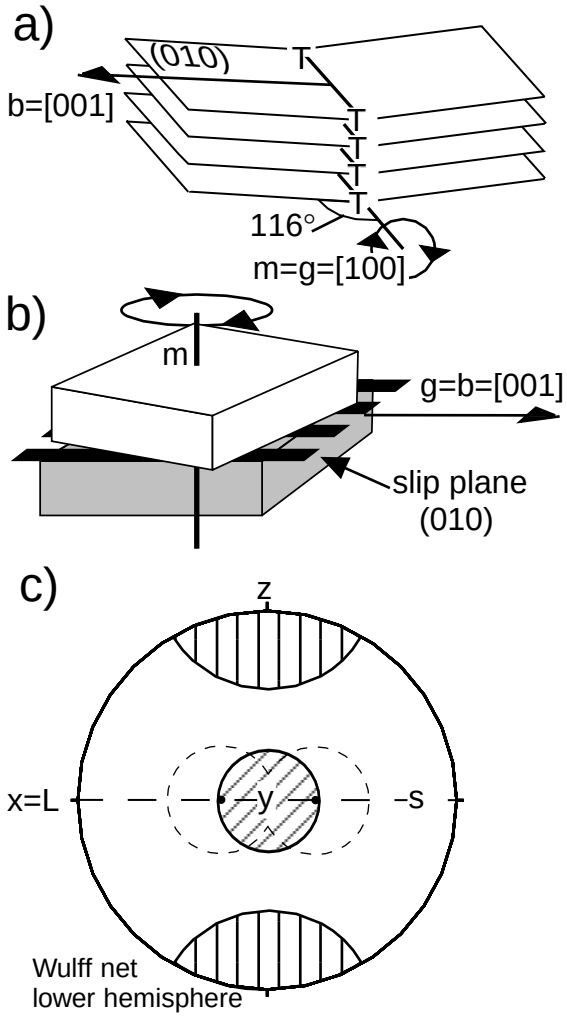

Fig. 3. (a) Schematic model of tilting of the crystal lattice due to arrangement of edge dislocations in a subgrain boundary. The misorientation is related to the slip system by the misorientation axis (m) which is parallel to the dislocation line $g = [100]$ within the slip plane (010). The Burgers vector $b = [001]$ of the edge dislocation is not perpendicular to the dislocation line (g). (b) Schematic model of twist boundaries due to arrangement of screw dislocations in the slip plane. The misorientation axis (m) is normal to the slip plane. The determination of Burgers vectors is not unique for twist-type misorientations, as all Burgers vectors normal to the misorientation axis are possible. (c) At high strains, the foliation plane rotates towards an end-orientation approximately parallel to the shear plane and therefore dislocation glide is most likely activated in slip planes parallel to the foliation with Burgers vectors parallel to the lineation. The perfect orientation for tilt-type misorientation axes related to the (010)[001] slip system is marked with dots and will be within the foliation plane at angles of 64 and 116° to the lineation (in (a), see text for explanation).Twist-type misorientation axis will be perpendicular to the foliation (z-axis). In terms of resolved shear stress, deviations from the perfect orientation will result in lower resolved shear stresses by the cosine of the angle between misorientation axis and the perfect orientations. 30° small circles around the perfect orientations represent the most likely areas for misorientation axes for tilt-type (dashed circles) and twist-type misorientations (resolved shear stresses >0.85 of the maximum, realized for the perfect orientations). For the case of tilt-type misorientations a central small circle around the y-axis (diagonal hatched) is chosen to simplify the selection of misorientation axes.

[001] is 116° (Deer et al., 1992) the angle between the misorientation axis and the Burgers vector differs from 90° (Fig. 3a) and in general may vary between about 60° and 120°. For screw dislocations the misorientation axis is perpendicular to all possible Burgers vectors within a slip plane. Therefore, misorientation axes perpendicular to the plane of a specific slip system can be attributed to screw dislocations on that slip system, while misorientation axes within a slip plane may result from edge dislocations on the specific slip system.

Considering the large number of possible slip systems in plagioclase and the measurement errors, the inverse pole figure alone usually does not yield a unique identification of a slip system for a given misorientation axis. Even the determination of twist or tilt relationships may be ambiguous. Therefore, further criteria are required. The slip systems activated should have a relatively high resolved shear stress, which is a function of the orientation of the slip plane and the slip direction with respect to the orientation of the applied stress tensor (Turner and Weiss, 1963; Poirier, 1985). The principal stress directions are not known in naturally deformed samples, but qualitatively it can be assumed that the orientations of active slip systems are suitably oriented for glide with respect to the kinematic framework in a shear zone. In the case of simple shear (which appears to have dominated the deformation in the present sample series) the axis of finite elongation (lineation) should approximate the shear direction, and the foliation, defined as the plane of mineral flattening, should be close to the shear plane at high strain. The direction of the greatest principal stress should lie at some angle to the shear plane and within the plane defined by the shear direction and the shear plane normal (simplified general stress field). Thus, slip planes parallel to the foliation with Burgers vectors parallel to the lineation are most suitably oriented for glide and should have the highest resolved shear stress (τ_{max}). Tilt-type misorientations caused by slip on the main slip system (010)[001] therefore will be expected to have rotation axes within the foliation at angles of 64 and 116° to the lineation (dots in Fig 3c). A tolerance angle of 30° around the two dots is arbitrarily chosen to represent the most probable location for tilt-type misorientation axes ($\tau_{rel} > 0.85$) (dotted circles in Fig. 3c). Other slip systems will have their favoured misorientation axes in a similar position or closer to the *y*-axis of the sample coordinate system. For the sake of simplicity, a small circle of 30° in the center of the pole figure is taken to represent the most reasonable location for tilt-type misorientations (diagonally hatched area in Fig. 3c). For twist boundaries, the misorientation axes are perpendicular to the slip plane (Fig. 3b) and thus to the foliation (parallel to the *z*-axis). The twist-type misorientation axes, which are related to slip systems characterized by high resolved shear stresses of $\tau_{rel} > 0.85$, will most probably be located within a small circle of ca. 30° around the *z*-axis (Fig 3c, vertically hatched area).

4. Results

4.1. Microstructural evolution observed by light microscopy

4.1.1. Sample of lowest deformation intensity

Some plagioclase porphyroclasts are strongly deformed and contain undulatory extinction, deformation bands, kink bands, as well as core-mantle structures with a rim of recrystallized grains (Fig. 4a). Other grains are intensely twinned. Three types of twins are identified: albite, pericline, and karlsbad twins (Fig. 4b). Most twins are tapered and bent and often do not terminate at grain boundaries (Fig. 4b), features that have been used to infer a deformation origin (Schmid, 1982) of albite and pericline twins (Kruhl, 1987b).

The recrystallized grains are usually not twinned. They represent 10–20% of the rock volume and do not form continuous layers. The size of the recrystallized grains is 40–100 μm (Fig. 4c). Grain boundaries and kink band boundaries are often serrated from bulging (migration) of the grain boundaries. The bulges have the same size as the subgrains, indicating that new grains have formed by a combination of subgrain rotation and local (slow) grain boundary migration (bulging recrystallization). Recrystallization also occurs in narrow bands crosscutting the porphyroclasts (Fig. 4c). Some of these bands may have initiated by fracturing or twinning. At the tips of non-penetrative bands (Fig. 4d) the plagioclase crystals are often highly strained (strong undulatory extinction, bent twins). Subsequent recrystallization of the highly strained zones or fractures may extend the band of recrystallized grains and may finally separate the plagioclase porphyroclasts into slices with high aspect ratio (Fig. 4c).

4.1.2. Sample of intermediate deformation intensity

The proportion of recrystallized grains increases with increasing deformation intensity. When there are approximately 25–30% of recrystallized grains, a macroscopic mineral lineation is detectable in hand specimen. Many porphyroclasts are strongly elongated and surrounded by a matrix of recrystallized grains (Fig. 5a). The recrystallized grain size is uniform and in the range of 40–100 μm. Most of the plagioclase porphyroclasts and recrystallized grains are polysynthetically twinned (Fig. 5b). Kink bands are common and are preferred sites of bulging recrystallization (Fig. 5b). Isolated small recrystallized grains on kink band boundaries are not twinned and thus may display lower internal strain, compared with the larger and probably older recrystallized grains in the recrystallized matrix which are usually twinned (see also Ji and Mainprice, 1990). Straight planar defects in highly elongated porphyroclasts display a step-like substructure at high magnifications (Fig. 5c). Some steps have segments parallel to (010) (albite twins) and segments roughly parallel to (001) (pericline twin), indicating translation parallel to the main slip system

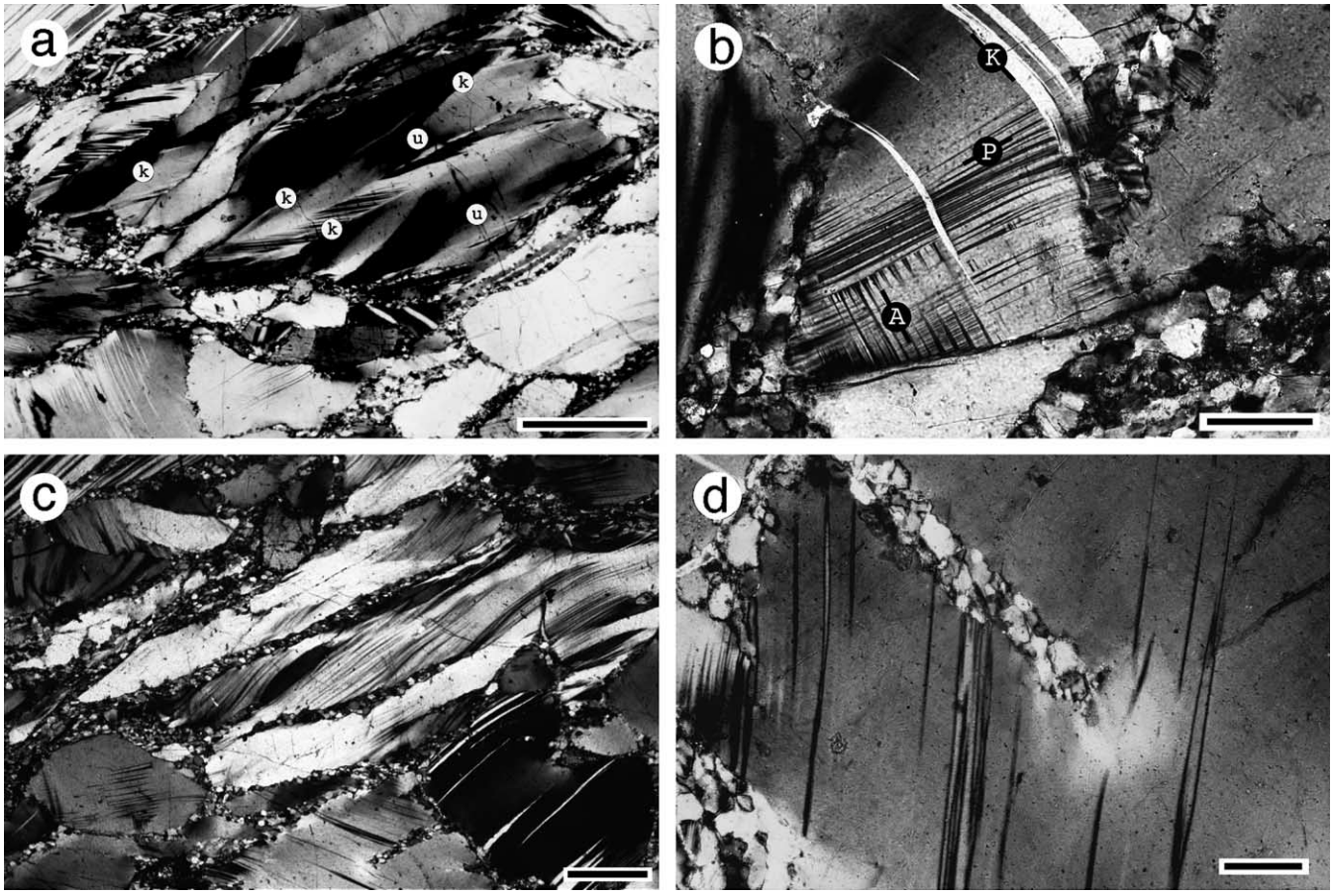

Fig. 4. Microstructures of the lowest deformation intensity. (a) Deformed plagioclase grains show undulatory extinction (u), and kink bands (k) (scale bar = 1 mm). (b) Deformation-induced twinning in plagioclase: albite twins (-A-), pericline twins (-P-) and karlsbad twins (-K-) (scale bar = 0.1 mm). (c) Core-mantle structure formed by recrystallization at the margin of primary plagioclase grains. Recrystallization on narrow bands crosscutting plagioclase porphyroclasts produces new elongated grains without a high amount of strain (scale bar = 1 mm). (d) Highly strained plagioclase crystal at the tip of a recrystallized band. Such bands may propagate through the porphyroclasts and dissect them (scale bar = 0.1 mm).

(010)[001]. However, some planar defects appear to be fractures. Recrystallized grains have formed along these planar defects (Fig. 5d). Some new grains appear to have formed by rotation recrystallization, but the origin of new grains along the fractures is not obvious from light microscope observations (Fig. 5d). Shear sense indicators are rare and only a few slightly asymmetric σ-clasts have been found which may be taken to indicate a sinistral shear sense in this sample.

Based on microstructural criteria, two populations of plagioclase porphyroclasts can be distinguished in this sample. The first, referred to as 'type-1 porphyroclasts', is characterized by high aspect ratios, straight grain boundaries, and polysynthetic albite twins at a low angle to the foliation plane (Fig. 5e). Type-1 porphyroclasts recrystallize at their margins and/or along narrow bands within the porphyroclasts oriented subparallel to the foliation plane (Fig. 5d and e). The second population, referred to as 'type-2 porphyroclasts', shows smaller aspect ratios and irregular grain boundaries (Fig. 5f). Albite twins are predominantly inclined at high angles to the foliation, and optically do not show a preferred orientation. Type-2 porphyroclasts are often strongly bent. Regions of recrystallized grains often extend far into the porphyroclasts, sometimes tapering into narrow zones, and produce the characteristic irregular grain shapes.

4.1.3. Sample of high deformation intensity

The portion of recrystallized grains increases with progressive deformation until porphyroclasts almost completely disappear. In the sample of the highest deformation intensity recrystallized plagioclase domains are dominated by equant recrystallized grains of 50–100 μm diameter and a few highly elongated porphyroclasts parallel to the mylonitic foliation. Porphyroclasts as well as recrystallized grains are twinned according to the albite, pericline and karlsbad laws.

Dynamic recrystallization has strongly modified the earlier microstructure in this sample. There are few relict structures from which the recrystallization processes can be inferred. Kinking of porphyroclasts is observed, but

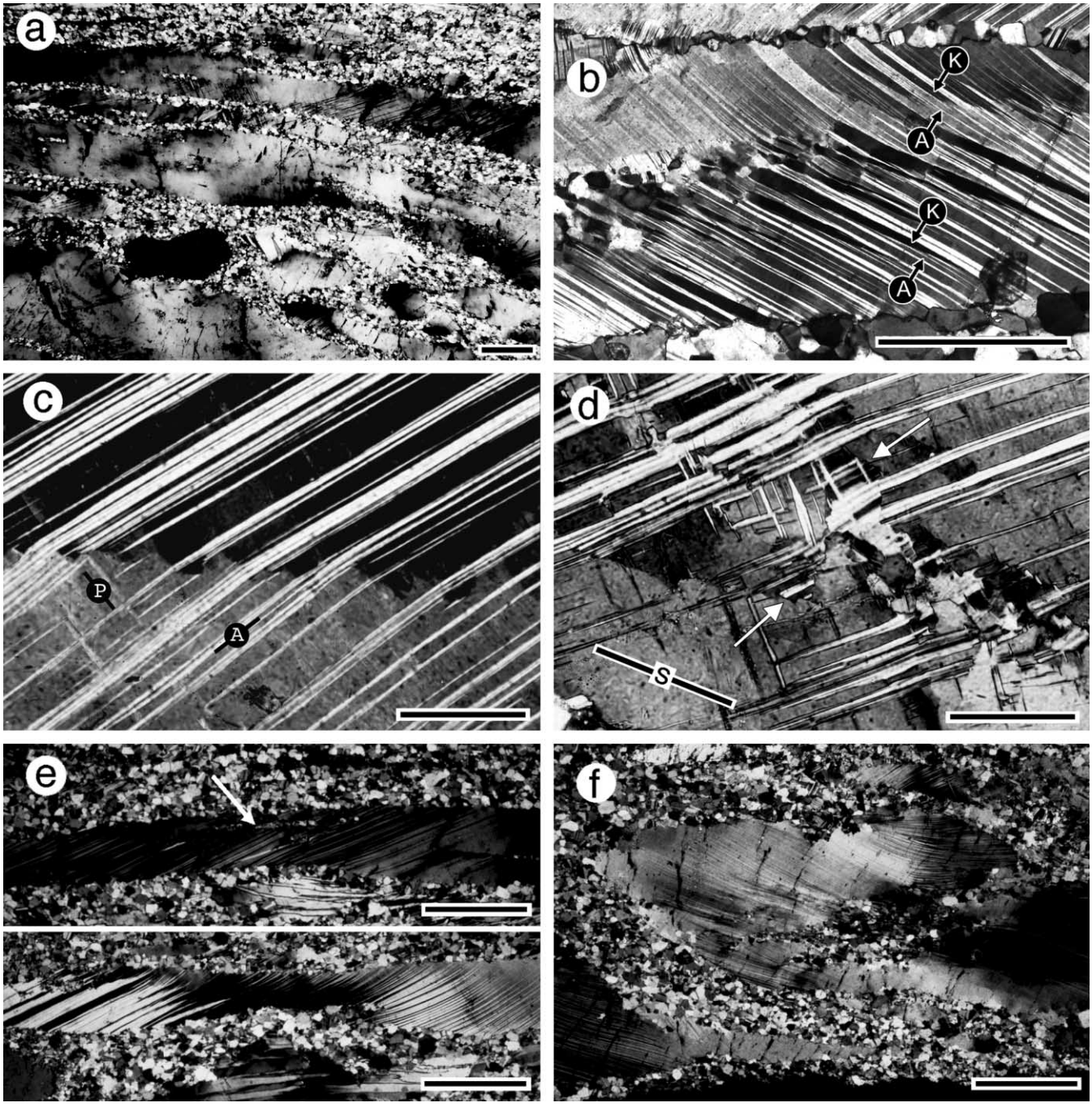

Fig. 5. Microstructures of intermediate deformation intensity (lineation and trace of foliation left–right if not indicated in the micrograph). (a) Plagioclase porphyroclasts within an interconnected matrix of recrystallized grains (scale bar = 1 mm). (b) Recrystallization on kink bands by bulging and subgrain rotation (upper margin). Karlsbad- (K) and albite twins (A) can be observed due to their different extinction. (scale bar = 0.5 mm). (c) Bending of the crystal lattice turns into a straight planar defect with a step-like substructure. Segments are roughly parallel to albite twins (010) (-A-) and parallel to pericline twins (001) (-P-), indicating translation on the (010)[001] slip system (scale bar = 0.1 mm). (d) Recrystallized grains in twinned and probably fractured porphyroclasts. Arrows mark planar defects, which most likely are fractures. New grains appear to be formed by some lattice rotation (related to twinning and subgrain rotation) as well as by other mechanisms (not identifiable by light microscopy) along planar defects (foliation as indicated, scale bar = 0.1 mm). (e) Type-1 porphyroclasts characterized by high grain shape anisotropy, straight grain boundaries, and polysynthetic albite twins subparallel to the foliation (scale bar = 1 mm). (f) Type-2 porphyroclasts characterized by less pronounced grain shape anisotropy, irregular grain shapes and albite twins at high angles to the foliation [(010) is inclined ca. 40° to the foliation] (scale bar = 1 mm).

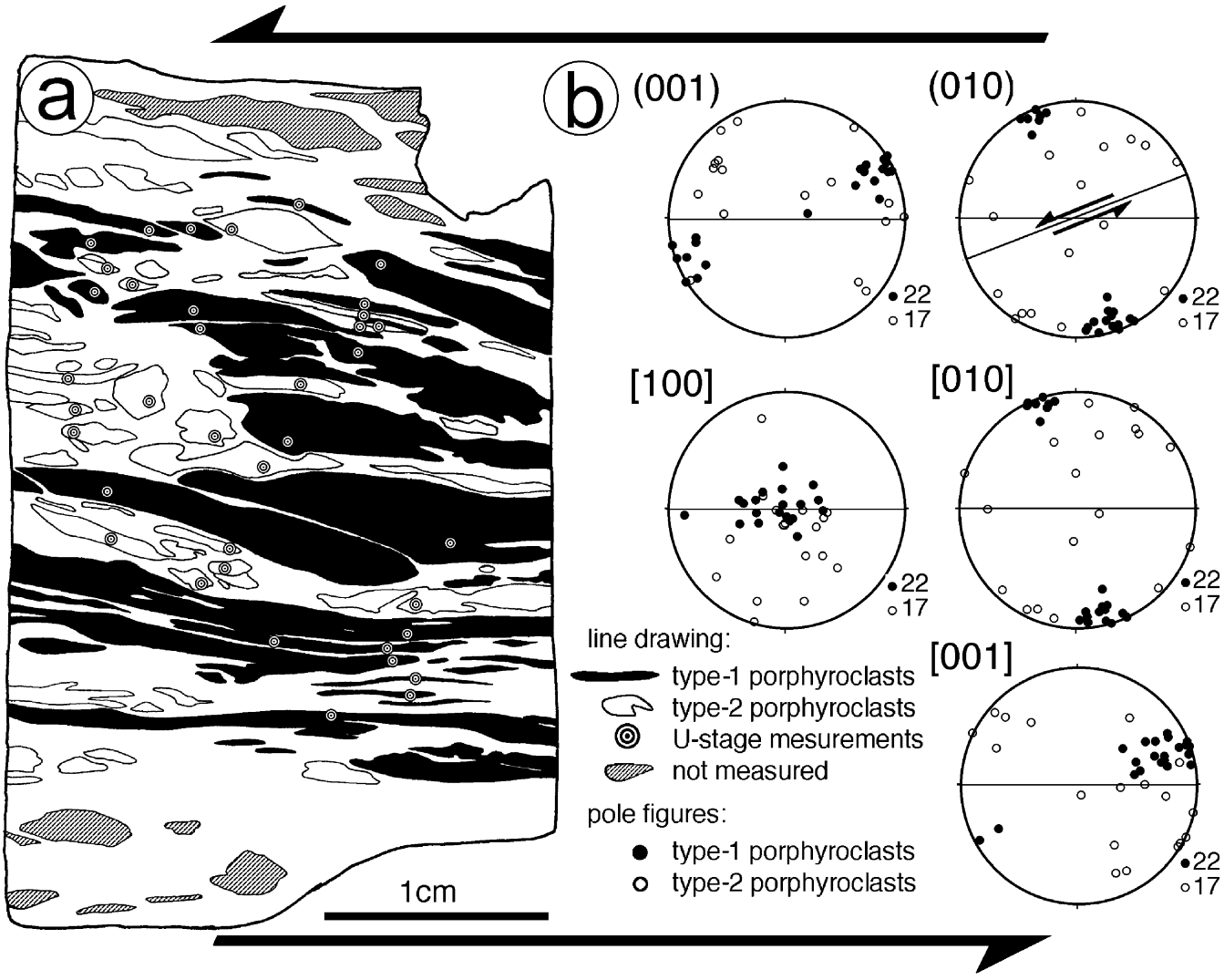

Fig. 6. CPO of plagioclase porphyroclasts from the sample of the intermediate deformation intensity. (a) Line drawing of the thin section; measured grains are marked with a dot; black: type-1 porphyroclasts, white: type-2 porphyroclasts. (b) Orientation of (001) and (010) poles and [100], [010] and [001] axes (foliation and lineation E–W in line drawings and pole figures; equal area projection lower hemisphere). The orientations of type-1 porphyroclasts (black) and type-2 porphyroclasts (white) largely do not overlap. Type-1 porphyroclasts are suitably oriented for slip on (010)[001] with respect to the oblique shear kinematics.

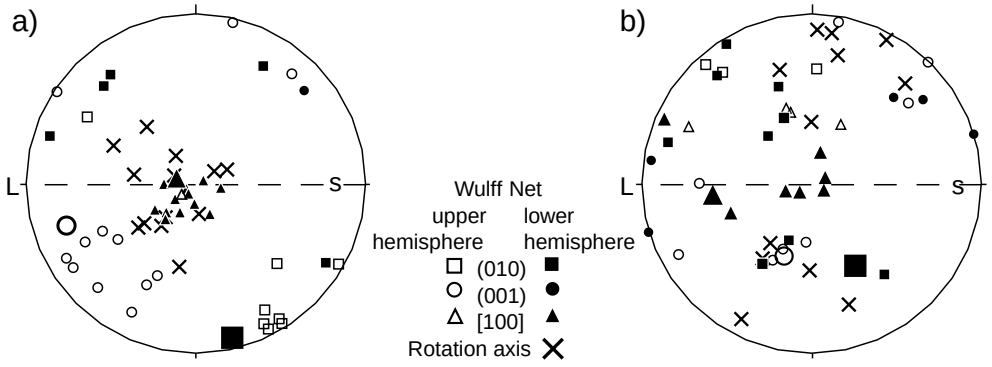

Fig. 7. Examples of orientations and misorientation axes of recrystallized grains within a single type-1 porphyroclast (a) and type-2 porphyroclast (b) (porphyroclast: large symbols, recrystallized grains: small symbols).

the kink band boundaries are already completely replaced by recrystallized grains. The previous distinction between the two types of plagioclase porphyroclasts can be applied to the most strongly deformed sample, but the microstructural differences of the two populations of porphyroclasts are not as clear as in the sample of intermediate deformation intensity.

4.2. Lattice preferred orientation and grain shape analysis of plagioclase porphyroclasts

The lattice preferred orientation (l.p.o.) of plagioclase porphyroclasts has been determined from petrographic thin sections of intermediate deformation intensity samples where the difference between the two types of porphyroclasts is most obvious. A line drawing of an entire thin section is given in Fig. 6a. The grain shapes and volume fractions of the porphyroclasts have been analyzed from the line drawing. The two populations of porphyroclasts show different orientation patterns (Fig. 6b). The preferred orientation of the type-1 porphyroclasts is characterized by well-defined maxima. The (010)-poles are inclined approximately 20° to the foliation plane and correspondingly the [001]-axes and the lineation enclose an angle of 20°. The (010)[001] slip system of plagioclase is oriented synthetically with respect to the sinistral shear sense in this sample. The resolved shear stress on the (010)[001] slip system is high in this orientation and therefore the type-1 porphyroclasts are in a favorable orientation for slip. The preferred orientation of the type-1 porphyroclasts thus may be interpreted to have formed by intracrystalline plastic deformation dominated by the (010)[001] slip system.

The orientation pattern of the type-2 porphyroclasts is more variable in all pole figures (Fig. 6b). Only very few porphyroclasts are oriented with their (010) planes subparallel to the foliation and [001]-axes close to the lineation. A few type-2 porphyroclasts show orientations of (001) ca. 30° inclined to the foliation and synthetic with respect to the sinistral shear sense (similar to (010) in type-1 porphyroclasts). Since (001) has been determined to be a possible slip plane in plagioclase by transmission electron microscopy (TEM) studies (Marshall and McLaren, 1977; Olsen and Kohlstedt, 1985), it is possible that dislocation glide may have been active on the (001)1/2[110] system in type-2 porphyroclasts.

In the least deformed sample the average aspect ratio of porphyroclasts is 2.3 ± 0.9 (long axes/short axes: mean value ± SD), and there is no visual difference between different types of porphyroclasts. In the sample of intermediate deformation intensity the aspect ratio of type-1 porphyroclasts is high; the mean value of 5.2 ± 3.2 is a minimum estimate because several grains are cut by the edge of the thin section. Crystal plasticity contributed to the grain elongation and significantly increased the aspect ratio compared with that of type-2 porphyroclasts of 3.5 ± 1.8, which is only a little higher than the anisotropy inherited from the earliest stages of deformation. The high aspect ratio of type-1 porphyroclasts, which correlates with a prominent l.p.o., suggests that it results from slip on (010)[001]. The orientation of the (010)[001] slip system is the most important difference between type-1 and type-2 porphyroclasts.

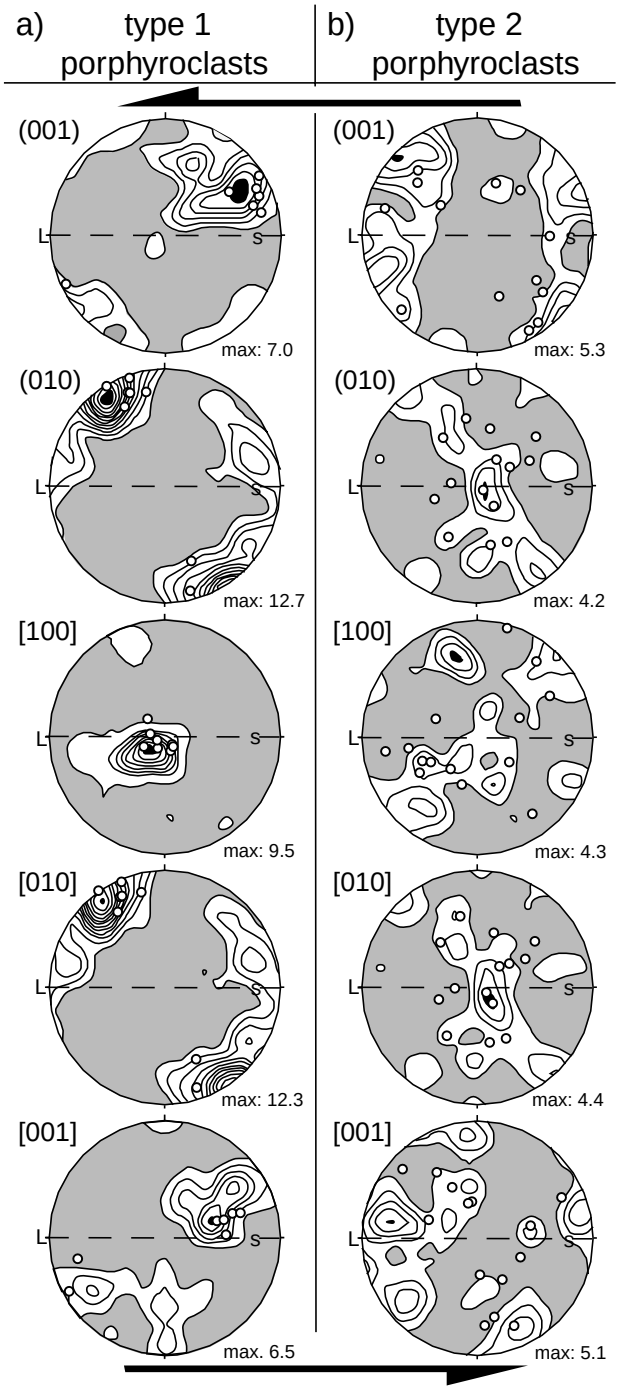

Fig. 8. CPO of porphyroclasts and recrystallized grains in: (a) type-1 porphyroclasts suitably oriented for easy slip on (010)[001] (eight porphyroclasts, 53 recrystallized grains); and (b) type-2 porphyroclasts unsuitably oriented for slip on (010)[001] (14 porphyroclasts, 54 recrystallized grains); contour lines: multiples of uniform, maximum black, <1 times uniform = shaded, Wulff net, lower hemisphere.

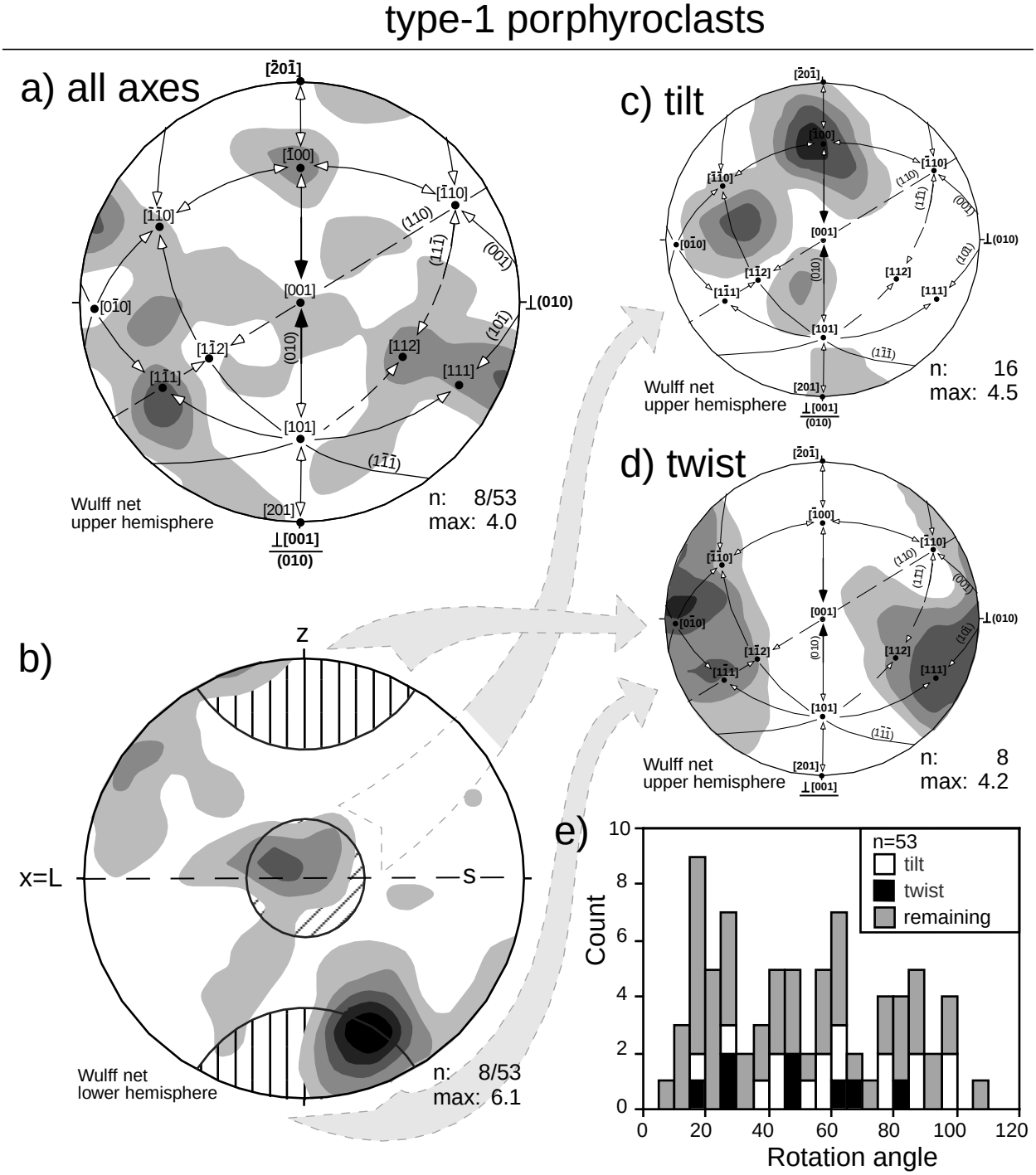

Fig. 9. Misorientation analysis of recrystallized grains within type-1 porphyroclasts. (a) Inverse pole figure of misorientation axes (*n*: numbers of porphyroclasts/number of misorientation axes). (b) Misorientation axis in specimen coordinate system, lineation and trace of foliation left–right (*x* parallel L, *y* normal to the projection plane, *z* perpendicular to the foliation *s*; diagonally hatched area: preferred site of tilt axes; vertically hatched: preferred site of twist axes, see Fig. 3c). (c) Tilt-type misorientation axes (*n*: number of misorientation axes). (d) Twist-type misorientation axes (*n*: number of misorientation axes). (e) Misorientation angles.

4.3. Misorientation analysis

The orientations of recrystallized grains in the two types of porphyroclasts have been measured in order to analyze the geometric relation between porphyroclasts and recrystallized grains (e.g. Fig. 5b, d and f). Only recrystallized grains in the interior of the porphyroclasts have been chosen because they are protected from overprinting of the initial orientation relationship by other processes such as grain boundary sliding, which has been inferred for the

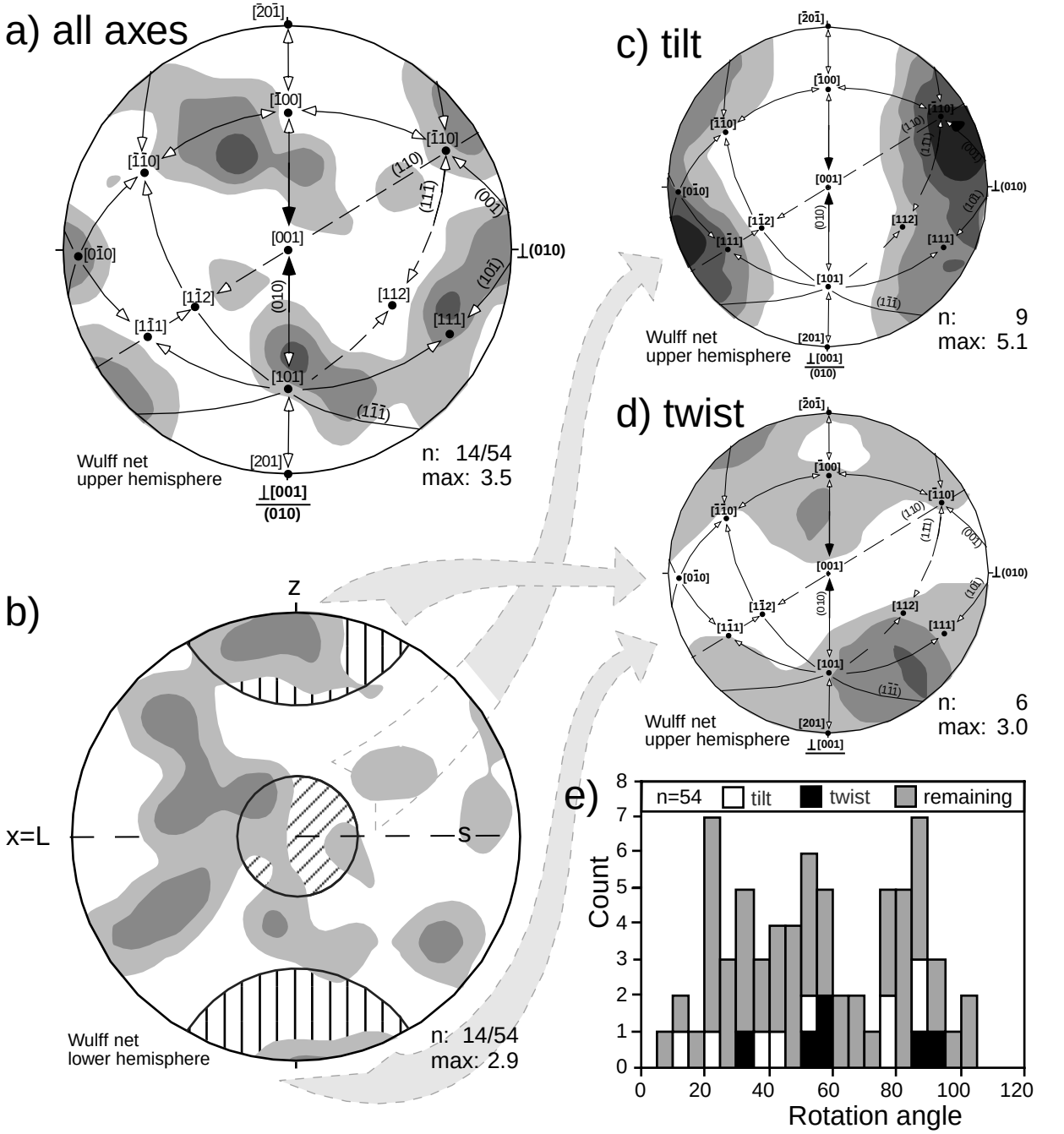

Fig. 10. Misorientation analysis of recrystallized grains within type-2 porphyroclasts. (a) Inverse pole figure of misorientation axes (*n*: numbers of porphyroclasts/number of misorientation axes). (b) Misorientation axis in specimen coordinate system, lineation and trace of foliation left–right (*x* parallel L, *y* normal to the projection plane, *z* perpendicular to the foliation *s*; diagonally hatched area: preferred site of tilt axes; vertically hatched: preferred site of twist axes, see Fig. 3c). (c) Tilt-type misorientation axes (*n*: number of misorientation axes). (d) Twist-type misorientation axes (*n*: number of misorientation axes). (e) Misorientation angles.

recrystallized matrix surrounding the porphyroclasts (Kruse and Stünitz, 1999).

An example of the orientation relationship of recrystallized grains within a type-1 porphyroclast is given in Fig. 7a and that of a type-2 porphyroclast in Fig. 7b. In the case of a type-1 porphyroclast, the crystallographic orientations of the recrystallized grains are similar to that of the porphyroclast. The misorientation angles are small and the rotation axes are clustered parallel to the *y*-axis of the sample coordinate system. Such an arrangement has been referred to as

'host control' (Vernon, 1975; Ji and Mainprice, 1990; Dornbusch, 1995). In the case of a type-2 porphyroclast (Fig. 7b) the recrystallized grains do not show a systematic orientation relationship with respect to the porphyroclast. The misorientation angles are large, and the corresponding axes are almost randomly distributed in the pole figure. Such arrangements have been referred to as 'no host control' (Jensen and Starkey, 1985; Olesen, 1987; Ji and Mainprice, 1990). The l.p.o. of all measured porphyroclasts (dots) and their recrystallized grains (contours) in Fig. 8 supports the distinction between 'host control' and 'no host control', although the larger scatter of porphyroclast orientations in the type-2 porphyroclasts makes the correlation of recrystallized grains and porphyroclasts more difficult.

Systematic analyses of the misorientation of recrystallized grains with respect to porphyroclast orientations have been performed for several porphyroclasts of both types (eight type-1 porphyroclasts, 14 type-2 porphyroclasts). The distribution of the misorientation axes in type-1 porphyroclasts shows some characteristic preferred orientations (Fig. 9). Misorientation axes plotted in the specimen reference system (Fig. 9b) show two maxima, the first indicative of tilting within a 30° small circle around the center of the pole figure, the second indicative of twisting within a 30° small circle around the pole to the foliation. The tilt-type misorientations are selectively presented in Fig. 9c and show three maxima, the main one parallel to the [100]-axis, and two weaker ones close to the $(1\bar{1}\,\bar{1})$-plane and some [uvw] orientation. The first maximum may be best explained by slip on (010)[001]. The other maxima are more difficult to relate to specific slip systems. Misorientation axes indicating twisting between porphyroclast and recrystallized grains are plotted separately in Fig. 9d, which shows a maximum at a high angle to (010). These misorientations can be inferred to be produced by slip on the (010) plane, probably on the main slip system (010)[001]. It can be concluded from the misorientation analysis of recrystallized grains and porphyroclasts that recrystallization in type-1 porphyroclasts occurs dominantly through progressive subgrain rotation involving slip on the (010)[001] slip system.

In type-2 porphyroclasts the relationship between porphyroclast and most of the recrystallized grains is not as clear (Fig. 10b). As in the example given in Fig. 7b, the distribution of all misorientation axes is almost random. This pattern illustrates that a distinct orientation relationship between porphyroclasts and recrystallized grains is only poorly developed. Only a few misorientation axes (nine out of 54) plot in the region indicative of tilt-type misorientations (Fig. 10b) and they are plotted separately in Fig. 10c. The broad maximum of misorientation axes is close to the $[\bar{1}10]$ axis and may be explained by glide on (001) with possible Burgers vectors [100] or $1/2[1\bar{1}0]$. A few misorientation axes may indicate slip on $(10\bar{1})$ with possible Burgers vectors parallel to [111]. Twist-type misorientations (six out of 54) are plotted separately (Fig. 10d). Only some of them may be related to the (001) slip plane. Since most of the misorientation axes between recrystallized grains and type-2 porphyroclasts cannot be clearly related to any slip system, it is concluded that recrystallization is probably not controlled by subgrain rotation related to a dominant slip system. Therefore, the mechanism of formation of new grains is different from type-1 porphyroclasts.

4.4. TEM observations

Three porphyroclasts with different orientations of their (010)[001] slip system have been selected from the intermediate deformation intensity sample for a TEM investigation to analyze dislocation densities and slip systems (Fig. 11). In porphyroclast 1, the slip plane and slip direction make a small angle with the foliation (shear plane) and lineation (shear direction; suitable orientation for slip on (010)[001], type-1-porphyroclast). In porphyroclast 2, the slip direction is oriented at a large angle to the shear direction ([001]-direction; not well oriented for slip on (010)[001], type-1-porphyroclast), and in 3, both the shear plane and shear direction, make a large angle with the shear plane and shear direction (unsuitably oriented for slip on (010)[001], type-2-porphyroclast). Slip systems have been identified by determining the Burgers vectors by invisibility criteria in bright and dark field (weak beam dark field, WBDF) modes. The crystallographic orientation of the dislocation lines has been determined by trace analysis after different tilt conditions (Hirsch et al., 1967, p. 312). The Burgers vector determination in conjunction with the

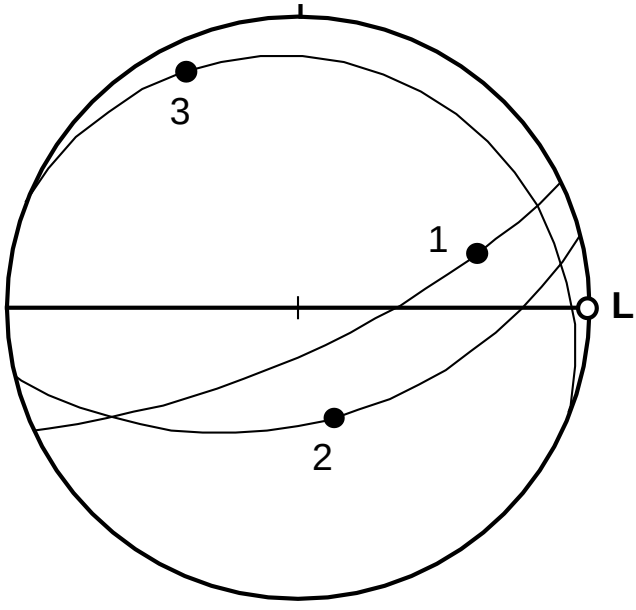

Fig. 11. Crystallographic orientation of the (010)[001] slip system of three porphyroclasts analysed in the TEM, given in the sample reference frame (horizontal line = foliation, L = lineation, lower hemisphere). The great circles indicate the orientation of the (010)-slip plane, the filled dots the orientation of the [001] slip direction.

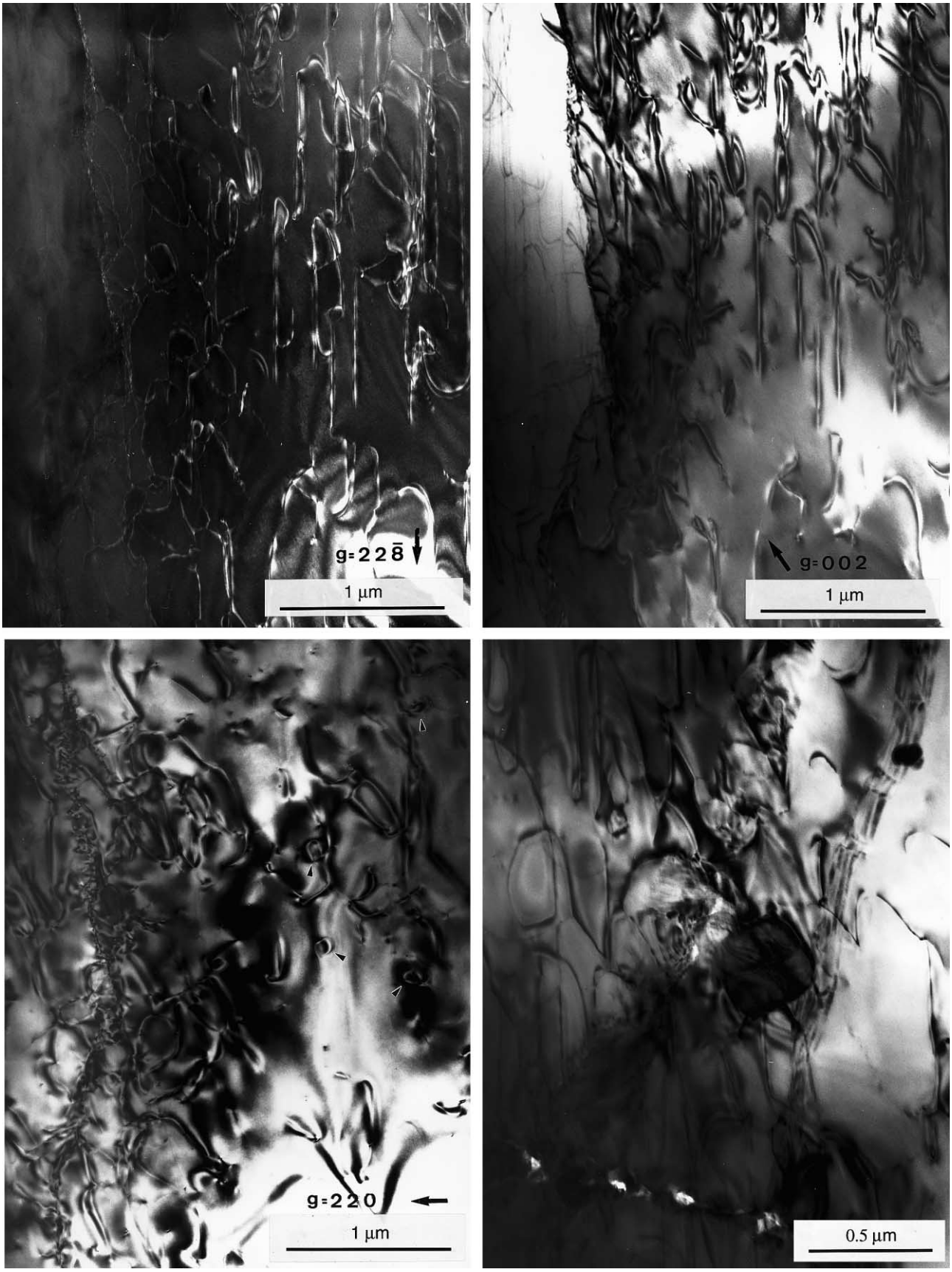
g=22$\bar{8}$
1 μm
g=002
1 μm
g=220
1 μm
0.5 μm

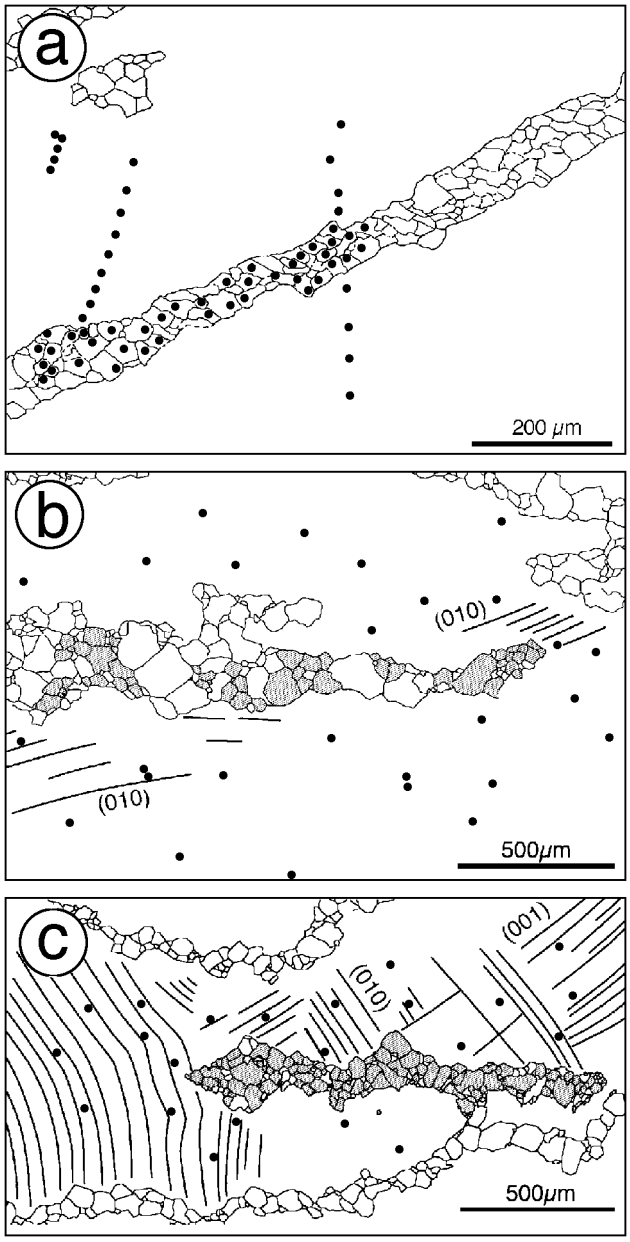

Fig. 13. Samples chosen for the determination of the chemical composition of porphyroclast and recrystallized grains in: (a) weakest deformed sample (central part of Fig. 4c); (b) intermediate deformed sample, type-1 porphyroclast; and (c) intermediate deformed sample, type-2 porphyroclast. Measured grains are hatched or marked with dots.

line orientations has been compared with the slip systems (Fig. 2) previously identified for the plagioclase $C\bar{1}$ structure (Marshall and McLaren, 1977; Olsen and Kohlstedt, 1984).

The types of dislocations, their distribution, and their slip systems do not vary systematically between the three different porphyroclasts. A series of micrographs of dislocations from porphyroclast 3 may serve as an example for the results of the slip system identification in the three porphyroclasts. All dislocations are visible in the WBDF image using $g = (22\bar{8})$ (Fig. 12a). The main set of north–south trending dislocations forming elongated loops is invisible using $g = (220)$ (Fig. 12b). The following set of known Burgers vectors is possible for the conditions of invisibility: [001], 1/2[1$\bar{1}$0], 1/2[1$\bar{1}$1], 1/2[1$\bar{1}$2]. Visibility of the north–south trending set of dislocations with $g = (22\bar{8})$, $(\bar{4}\,\bar{4}4)$, $(\bar{2}\,\bar{2}4)$ rules out 1/2[1$\bar{1}$0], and leaves [001], 1/2[1$\bar{1}$1] and 1/2[1$\bar{1}$2] as possible Burgers vectors for this set of dislocations. The [1$\bar{1}$1] Burgers vector lies in the (10$\bar{1}$)-plane. The north–south dislocation line orientation is [001], and this line orientation is not contained in the (10$\bar{1}$)-plane, so that [1$\bar{1}$1] is not a possible solution; [1$\bar{1}$2] is only a tentative Burgers vector, and the most probable Burgers vector solution for this set of dislocations is [001]. The dislocation line [001] operates in (*hk*0), most importantly in (010) (Marshall and McLaren, 1977). The line direction [001] indicates that the long segments of these dislocations are screw segments. Many of these dislocations form loops with long screw and short 'edge' segments. The other set of more irregular dislocations and small round loops (arrows in Fig. 12b) is invisible with $g = (002)$, which only leaves 1/2[110] and 1/2[1$\bar{1}$0] as possible Burgers vectors. Visibility of this set with $g = (22\bar{8})$ (Fig. 12a) rules out 1/2[1$\bar{1}$0] and only leaves 1/2[110] as the Burgers vector, operating in the (001)- or $(1\bar{1}\,\bar{1})$-plane. The subgrain boundary in the images consists of both sets of dislocations (Fig. 12a–c).

The other two porphyroclasts show similar results, with (010)[001] as the main slip system, long screw segments, dipoles and elongated loops of [001] dislocations, and more irregular [110]-dislocations. The dislocation densities do not vary systematically between the different porphyroclasts: $\rho = 8 \times 10^8\,\mathrm{cm}^{-2}$ in porphyroclast 1, $\rho = 1 \times 10^9\mathrm{z}\,\mathrm{cm}^{-2}$ in porphyroclast 2, and $\rho = 8 \times 10^8\,\mathrm{cm}^{-2}$ in porphyroclast 3. Thus, (010)[001] and (001)1/2[110] or $(1\bar{1}\,\bar{1})$1/2[110] are the important slip systems in all three plagioclase porphyroclasts, regardless of the orientation of these slip systems with respect to the kinematic framework.

Microfractures are common in porphyroclast 3 (Fig. 12d), whereas no microfractures have been observed in the other two clasts, where twins and subgrain boundaries are the only planar defects. Dislocations and some porosity are observed along these fractures. Small grains of ilmenite have been identified by analytical TEM along the fractures (Fig. 12d). In the light microscope, ilmenite usually is found along

Fig. 12. TEM images of porphyroclast 3 in Fig. 11. (a) to (c) show the same area under different diffraction conditions. (a) Weak beam dark field image showing most dislocations visible and a subgrain boundary in the left part of the area. $g = 22\bar{8}$. (b) Only one set of largely parallel dislocations of (a) is visible with $g = 002$. (c) The other set of dislocations, which are invisible in (b), is visible with $g = 220$, also small loops of dislocations (arrows). The set of largely parallel dislocations of (b) is invisible under these diffraction conditions. (d) Three fractures (between arrows) intersect near the center of the image and a new grain of ilmentite (dark) has nucleated in the region of the intersection. Note the porosity along the fracture in the left part of the image and near the center.

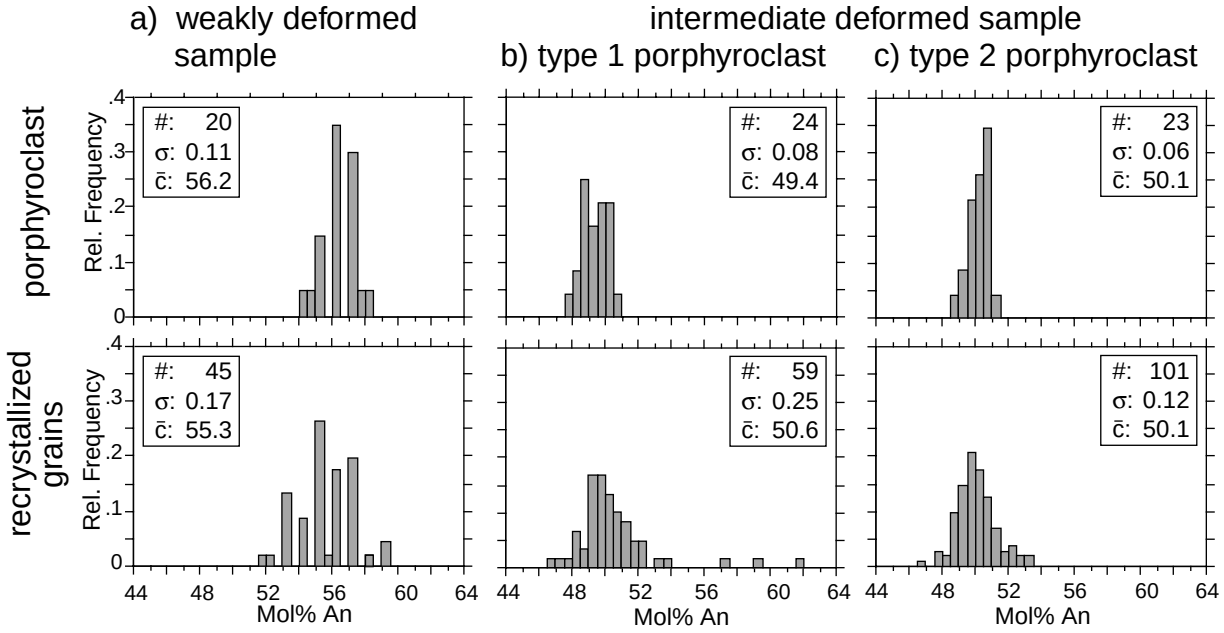

Fig. 14. Chemical composition of plagioclase porphyroclasts and recrystallized grains displayed in Fig. 13. (a) Weakest deformed sample; (b) intermediate deformed sample, type-1 porphyroclast; and (c) intermediate deformed sample, type-2 porphyroclast.

some grain boundaries and inside plagioclase and hornblende grains in the vicinity of brown hornblende porphyroclasts, which recrystallize to greenish hornblende during the mylonitization. The green hornblende contains less Ti and Fe than brown hornblende (see analyses in Table 1 of Kruse and Stünitz, 1999), accounting for the formation of ilmenite during the compositional change and recrystallization of hornblende. The crystallization of ilmenite along fractures in plagioclase suggests that these fractures probably formed during the mylonitization, when the ilmenite formed from the break-down of brown hornblende.

4.5. Chemical composition

The chemical compositions of plagioclase porphyroclasts and recrystallized grains have been analyzed in the samples with the weakest and intermediate deformation intensity. The line drawings of the sites chosen for microprobe measurements (Fig. 13) are based on electron backscatter images. The twin planes have been identified on the U-stage.

In the sample with the weakest deformation intensity (Fig. 13a), the anorthite content of porphyroclasts (An 56) and recrystallized grains (An 55) is the same within the range of error of microprobe measurements (Fig. 14a). The range of compositions is twice as large in recrystallized grains ($\Delta An = 7.4$) compared with porphyroclasts ($\Delta An = 4$) (Fig. 14a). In the sample with the intermediate deformation intensity, two porphyroclasts have been measured; the first is a porphyroclast suitably oriented for slip on (010)[001] (Fig. 13b; type-1 porphyroclast), whereas the second one is unsuitably oriented for slip on (010)[001] (Fig. 13c; type-2 porphyroclast). In both examples the mean chemical composition is the same (An 50) for both porphyroclasts and recrystallized grains. Only the range of recrystallized grains (Fig. 14b) is twice as large as in the porphyroclasts (omitting the measurements of $An > 56$) (Fig. 14c).

5. Discussion

Dynamic recrystallization as defined by Poirier and Guillopé (1979) is a process that leads to a reconstitution of the crystalline material without a major change in chemical composition (driven only by internal strain energy). However, chemical reactions may occur simultaneously with dynamic recrystallization (Etheridge and Hobbs, 1974; Tullis, 1983; Yund and Tullis, 1991; Stünitz, 1998). Compositional changes during the recrystallization of plagioclase have been commonly observed and may be correlated with prograde or retrograde metamorphic reactions during the deformation (White, 1975; Brown et al., 1980; Sondre Borges and White, 1980; Brodie, 1981; Olsen and Kohlstedt, 1985; Molli, 1994; Stünitz, 1998). The mean values of the anorthite content of porphyroclasts and recrystallized grains in our analyzed samples do not change within the range of error. Thus, the recrystallization is truly dynamic in the sense of Poirier and Guillopé (1979).

The different orientation patterns of the two populations of porphyroclasts correspond to ‘soft’- (suitably oriented for slip on (010)[001]; type-1 porphyroclasts) and ‘hard’-orientations (unsuitably oriented for slip on (010)[001]; type-2 porphyroclasts). During recrystallization of the two

types of porphyroclasts, different recrystallization microstructures and misorientation patterns have been produced. The results from the misorientation analysis can be summarized as follows:

1. In type-1 porphyroclasts most of the misorientation axes are related to tilt or twist on the (010)[001] slip system of plagioclase (Fig. 9). The recrystallization process results in a host control relationship between porphyroclasts and recrystallized grains and is inferred to be progressive subgrain rotation.
2. In type-2 porphyroclasts very few misorientation axes can be related to known slip systems. Slip on (010), (001), and (10 − 1) may have occurred, but most orientation relationships between porphyroclasts and recrystallized grains cannot be explained by progressive subgrain rotation.

Different orientations of crystals and their slip systems with respect to the principal stress directions may cause the activation of different slip systems and may result in different dislocation densities, affecting the recrystallization process. However, the results of the TEM analysis show that the same slip systems are activated in both types of porphyroclasts and dislocation densities do not differ systematically. Thus, different dislocation densities and activation of different slip systems are not responsible for the different recrystallization microstructures of the two types of porphyroclasts.

The question arises: what is the dominant process that is responsible for the recrystallization of type-2 porphyroclasts? Grain boundary migration could account for the no-host control misorientation relationships of type-2 porphyroclasts, but does not generate new and necessarily smaller grains. Large rotation angles between porphyroclasts and recrystallized grains have been observed in plagioclase (Fitz Gerald et al., 1983), olivine (Avé Lallemant, 1985) and metals and ceramics (Escher and Gottstein, 1998; Randle, 1992, 1993). Avé Lallemant (1985) proposed that grain boundary migration starting from nuclei in submicroscopic shear bands may be responsible for such orientation relations. Similar processes have been inferred from in-situ TEM observations on Ni_3Al during annealing experiments (Escher and Gottstein, 1998). Thus, it seems that at sites of stress concentrations, local high defect densities allow the nucleation of new grains without a host control relationship. In our samples, only porphyroclasts in 'hard' orientations for the dominant (010)[001] slip system (type-2 porphyroclasts) show extensive microfracturing. Otherwise, the TEM substructures between 'soft' and 'hard' orientations are identical, and both show evidence for dislocation climb. The 'hard' orientations have lower aspect ratios and are therefore less deformed, but they must have been subjected to higher stresses during deformation so that fracturing is more likely than in 'soft' orientations (type-1 porphyroclasts). It appears that some recrystallization takes place along former fractures, and zones of recrystallized grains extend along fracture-like structures in porphyroclasts. Along microfractures, small, nearly strain-free fragments may have passively rotated and serve as nuclei for new grains. The boundaries of small and strain-free nuclei may migrate into the surrounding material, because the vicinity of cracks usually contains high defect densities and elastically strained crystals (Fitz Gerald et al., 1991; Fitz Gerald and Stünitz, 1993; McLaren and Pryer, 2001). Thus the driving potential for the boundary migration is strain energy. The orientation relationships that may develop are defined by the orientations of the nuclei produced during fracturing, which may have high misorientation angles and irrational misorientation axes (Escher and Gottstein, 1998).

New grains nucleating along fractures have been observed in plagioclase deformed at low temperatures by Fitz Gerald and Stünitz (1993), but nucleation in those examples was largely driven by chemical disequilibrium. In the samples of this study, there is no compositional change between recrystallized grains and porphyroclasts, and recrystallization was only driven by strain energy. Fracturing in feldspar has been observed at high deformation temperatures (Tullis, 1983; Fitz Gerald and Stünitz, 1993, and references therein) and its importance for plagioclase deformation is well established (Tullis and Yund, 1985, 1987). Pre-fractured albite samples undergo preferential recrystallization along the fracture surfaces and continue to deform by recrystallization accommodated dislocation creep (Tullis et al., 1990). The effect of fracturing on dislocation activity and thus crystal plastic deformation has been pointed out by Fitz Gerald et al. (1991) and McLaren and Pryer (2001). Our results from misorientation analysis and TEM substructures suggest that fracturing in plagioclase is important for the recrystallization process during dominantly crystal plastic deformation and may explain the observation of no-host control orientation relationships between porphyroclasts and recrystallized grains.

6. Conclusions

Two types of porphyroclasts can be distinguished in the investigated mylonitic anorthosites: type-1 porphyroclasts show high aspect ratios and have the (010)[001] slip system suitably oriented for slip in the kinematic reference frame of the crystals; type-2 porphyroclasts show smaller aspect ratios and have the (010)[001] slip system unsuitably oriented for slip. The dislocation substructures and densities are very similar in the two types of porphyroclasts regardless of their crystallographic orientation with respect to the kinematic framework. The most important slip systems, in terms of dislocations, in all porphyroclasts are (010)[001] $1/2\langle 110\rangle$ in (001) or $\{1\bar{1}\,\bar{1}\}$. The dominant recrystallization process in type-1 plagioclase porphyroclasts is subgrain rotation recrystallization, which leads to formation of new

grains that preserve a characteristic crystallographic orientation relationship with respect to the porphyroclasts, even at higher misorientation angles (host control).

In type-2 porphyroclasts microfractures are common and appear to be important for the nucleation of new grains. The formation of new grains occurs in regions of high defect density, e.g. along fractures. Thus, microfracturing may be a process for forming nuclei during dynamic recrystallization in plagioclase. New grains formed by microfracturing may grow by subsequent grain boundary migration. The misorientations between recrystallized grain and porphyroclast developed by this process are arbitrary and show no host control orientation relationships between porphyroclasts and recrystallized grains.

TEM and misorientation analysis yield results for the determination of slip systems that are largely consistent. Misorientation analyses may produce large errors for the direction of misorientation axis if the misorientation angles are small and if the accuracy of the measured crystallographic orientations exceeds a level of 1–2°. This accuracy requirement is independent of the measuring equipment.

Acknowledgements

We thank Renee Heilbronner, Stefan Schmid and David Mainprice for stimulating discussions. The manuscript has been improved substantially by the very constructive reviews of Jan Tullis and an anonymous reviewer. This work has been supported by NF grant Nos. Swiss National Funds 20-49562.96 and 2000-055420.98.

Appendix A. Error estimation for misorientation axes

The uncertainty in obtaining the pole (hkl) or direction [uvw] of a misorientation axis depends on the misorientation angle and the accuracy of the applied technique for orientation measurements (Fitz Gerald et al., 1983). The error for the axis increases with decreasing misorientation angle and decreasing orientation accuracy.

A graphical solution to quantify the error of determining the misorientation axes is illustrated for a simplified case between two directions on the sphere (Fig. A1). The directions 1 and 2 (representing the axes $[uvw]_1$ and $[uvw]_2$ of two crystals) can be transferred into each other by a rotation about a fixed axis and angle. This axis/angle-pair is not unique; the rotation angle can assume values between the angular distance θ of both directions and 180°, corresponding to various rotation axes on the bisecting great circle b of equal distance to directions 1 and 2. Here we consider as the misorientation between 1 and 2 the (unique) rotation with the minimum angle θ and the axis R perpendicular to both 1 and 2.

Let the accuracy of the measurements be given by a small circle r around the measured directions 1 and 2. For directions within these small circles r the rotation axis will deviate from R on b. The largest deviation δ_{max} will occur for some directions on a tangent t to both small circles r as shown in Fig. A1, where the rotation axis lies on a great circle b_e perpendicular to t. A solution for δ_{max} is derived by spherical trigonometry:

$$\sin\delta_{max} = \sin r/\sin(\theta/2) \quad \text{(A1)}$$

As the above equation was derived geometrically for the misorientation between two directions (axes), a very similar equation holds true for the misorientation between two (crystallographic) orientations as proper rotations of the crystal lattice with respect to a fixed reference frame. Analogous to directions as elements of the unit sphere $S^3 \subset R^3$ in three-dimensional space, orientations can be

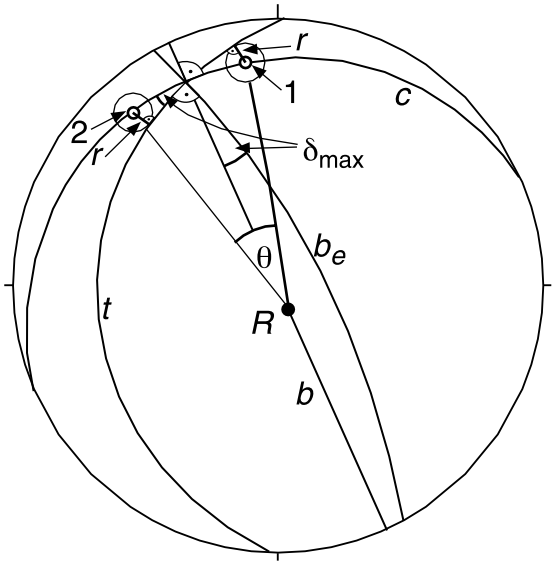

Legend:

1,2	orientation measured on the u-stage
r	measurement accuracy as small circle around 1,2
c	great circle around *R* through 1 and 2
b	bisectrix to 1,2
R	rotation axis on *b*
θ	rotation angle between 1 and 2 around *R*
t	tangent to the the small circles *r* of 1,2
δ_{max}	maximum deviation from *b*
b_e	great circle perpendicular to *t*; rotation axis charged with maximum error will lay on b_e

Fig. A1. Graphical illustration of the variation in misorientation axis between two directions 1 and 2 of given misorientation angle θ with measurement errors r.

represented by quaternions as elements of the unit (half) sphere $S^4_+ \subset R^4$ in four-dimensional space (for details see Altmann (1986), Kunze (1991) and Schaeben (1996)). The quaternion Q is related to the rotation angle ω and rotation axis **n** of the orientation by:

$$Q = [\cos(\omega/2),\ \mathbf{n}\sin(\omega/2)] \tag{A2}$$

Let Q_1 and Q_2 represent two orientations of grains 1 and 2. There is exactly one quaternion Q_0 with shortest (and equal) distance ω_m to both of them such that:

$$Q_1 = Q_m Q_0 \ \text{ and } \ Q_2 = Q_m^{-1} Q_0 \tag{A3}$$

where Q_m is related to the misorientation $Q_1 Q_2^{-1}$ between grains 1 and 2 with misorientation angle $\omega_{12} = 2\omega_m$ by:

$$Q_m^2 = [\cos(\omega_m), \mathbf{n}_m \sin(\omega_m)] = Q_1 Q_2^{-1} \tag{A4}$$

For the sequence of rotations the rules of quaternion multiplication apply, and the inverse to a quaternion is given by the negative rotation axis:

$$Q^{-1} = [\cos(\omega/2),\ -\mathbf{n}\sin(\omega/2)] \tag{A5}$$

Now both orientations 1 and 2 are measured with an uncertainty, say within a tolerance of rotation angle ω_r with arbitrary rotation axis. Then the measured orientations will be represented by modified quaternions $\underline{Q}_{1,2}$

$$\underline{Q}_1 = Q_r Q_1 = Q_r Q_m Q_0, \qquad \underline{Q}_2 = (Q_r Q_m)^{-1} Q_0, \qquad \underline{Q}_1 \underline{Q}_2^{-1} = (Q_r Q_m)^2 \tag{A6}$$

where the term for $\underline{Q}_2$ was chosen by symmetry arguments to maximize the resulting deviation between the rotation axes of $Q_1 Q_2^{-1}$ and $\underline{Q}_1 \underline{Q}_2^{-1}$. This deviation δ is the angle between the (true) rotation axes $\mathbf{n}_m$ of Q_m and the (measured) rotation axis **n** of $Q_r Q_m =: Q$, which is given by:

$$\cos(\omega/2) = c_m c_r - \mathbf{n}_m \times \mathbf{n}_r s_m s_r$$
$$\mathbf{n}\sin(\omega/2) = \mathbf{n}_r c_m s_r + \mathbf{n}_m s_m c_r - \mathbf{n}_m \times \mathbf{n}_r s_m s_r \tag{A7}$$

(where $c_i = \cos(\omega_i/2)$ and $s_i = \sin(\omega_i/2)$ for $i = m,r$). The deviation δ results from:

$$\cos\delta = \mathbf{n}_m \times \mathbf{n} = [c_r - c_m \cos(\omega/2)]/[s_m \sin(\omega/2)] \tag{A8}$$

The maximum deviation δ_{max} follows by differentiation after ω according to:

$$d(\cos\delta)/d\omega = 0 \qquad \cos(\omega_{max}/2) = c_m/c_r$$
$$\cos\delta_{max} = (c_r^2 - c_m^2)^{1/2}/s_m \tag{A9}$$

and finally:

$$\delta_{max} = \text{asin}[\sin(\omega_r/2)/\sin(\omega_{12}/4)] \ \ (2\omega_r \le \omega_{12}) \tag{A10}$$

This result matches Eq. (A1) when identifying $\omega_r/2$ and $\omega_{12}/2$ with r and θ, respectively. The approximation $\sin(\omega) \approx \omega$ for small angles ($<10°$) gives $\delta_{max} \approx 2\omega_r/\omega_{12}$ for orientations and $\delta_{max} \approx 2r/\theta$ for directions, respectively, where angles are given in radians. For errors ω_r larger than half the misorientation angle ω_{12}, the maximum deviation δ_{max} hits the upper limit of 90° possible for the angle between two misorientation axes (Eq. (A10)).

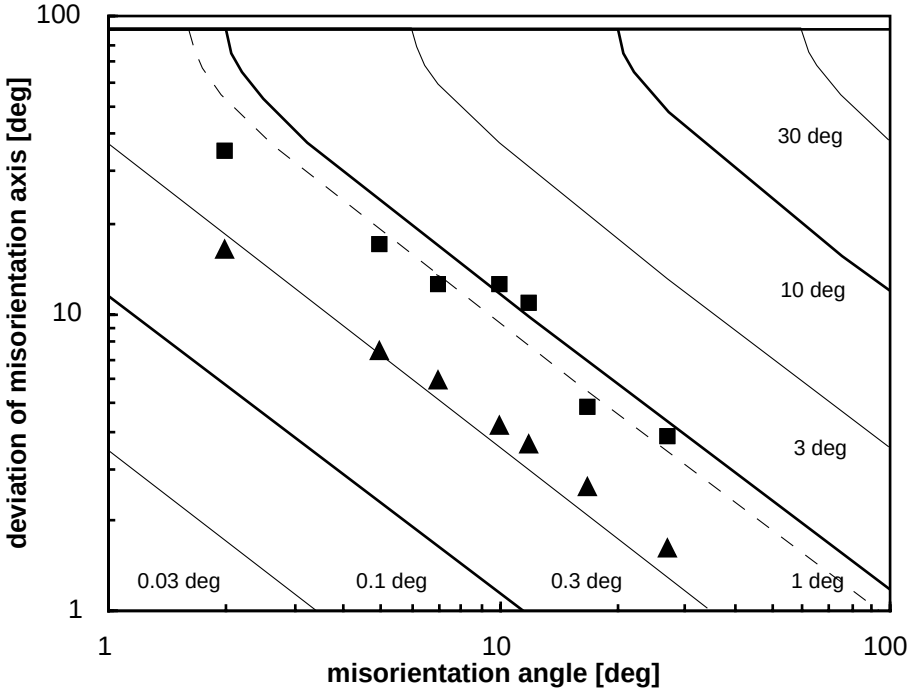

Fig. A2. Maximum deviation δ_{max} of the misorientation axis as function of the misorientation angle ω_{12} (2θ) for different accuracy levels ω_r ($2r$) of orientation measurements in logarithmic scale. Data from Prior (1999) for maximum (squares) and average (triangles) deviation from best rotation axis marked, with matching curve for orientation precision of 0.8° superimposed (dashed).

The necessary precision ω_r to measure two orientations 1 and 2 is approximately half the product of their misorientation angle ω_{12} and the allowed maximum error δ_{max} for the rotation axis to be derived. For example, if the rotation axis is needed within a maximum error of 1° (10°), then the two orientations would have to be measured with a precision of a hundred (ten) times smaller than their actual misorientation angle. The accuracy of U-stage measurements is about 2–3° (Siegesmund et al., 1994), which propagates to possible deviations of 24–37° for the misorientation axis for a misorientation angle of 10°. The accuracy of EBSD measurements is somewhat higher (about 1° for absolute orientations; Trimby et al., 1998), but misorientations with angles less than 5° still may involve considerable errors in the misorientation axis (24° and more).

It must be mentioned that the derived Eqs. (A1) and (A10) yield the maximum error in a sense of a true upper bound. For a statistical population of many misorientations based on orientation measurements with random errors, the standard deviation for the rotation axis is certainly smaller. Prior (1999) found experimentally on a data set for 30 garnet grains that the average deviation of the misorientation axis from the best constrained axis was one third to one half of the maximum deviation. Prior's data for the maximum deviation fit well with the above relation (Fig. A2) and correspond to a very reasonable estimate for his EBSD precision (random error of absolute orientation measurements) of about 0.8°.

References

Altmann, S.L., 1986. Rotations, Quaternions and Double Groups. Oxford University Press, Oxford, 317pp.

Avé Lallemant, H.G., 1985. Subgrain rotation and dynamic recrystallization of olivine, upper mantle diapirism, and extension of the Basin-and-Range Province. Tectonophysics 119, 89–117.

Bell, T.H., Johnson, S.E., 1989. The role of deformation partitioning in the deformation and recrystallization of plagioclase and K-feldspar in the Woodroffe Thrust mylonite zone, central Australia. Journal of Metamorphic Geology 7, 151–168.

Benn, K., Mainprice, D., 1989. An interactive program for determination of plagioclase crystal axes orientations from u-stage measurements: an aid for petrofabric studies. Computers and Geosciences 15, 1127–1142.

Boullier, A.M., Gueguen, Y., 1975. SP-Mylonites: origin of some mylonites by superplastic flow. Contribution to Mineralogy Petrology 50, 93–104.

Brodie, K.H., 1981. Variations in amphibole and plagioclase composition with deformation. Tectonophysics 78, 385–402.

Brown, W.L., Macaudière, J., Ohnenstetter, M., 1980. Ductile shear zones in a meta-anorthosite from Harris, Scottland: textural and compositional changes in plagioclase. Journal of Structural Geology 2, 281–287.

Buatier, M., van Roermund, H.L.M., Drury, M.R., Lardeaux, J.M., 1991. Deformation and recrystallization mechanisms in naturally deformed omphacites from the Sesia–Lanzo zone; geophysical consequences. Tectonophysics 195, 11–27.

Bunge, H.J., 1985. Representation of preferred orientations. In: Wenk, H.R. (Ed.). Preferred Orientation in Deformed Metals and Rocks: An Introduction to Modern Texture Analysis. Academic Press, Orlando, pp. 73–108.

Burg, J.P., Wilson, C.J.L., Mitchell, J.C., 1986. Dynamic recrystallization and fabric development during the simple shear deformation of ice. Journal of Structural Geology 8, 857–870.

Burri, C., Parker, R., Wenk, E., 1967. Die optische Orientierung der Plagioklase. Birkhäuser, Basel 334pp.

Cahn, R.W., 1983. Recovery and recrystallization. In: Cahn, R.W., Haasen, P. (Eds.). Physical Metallurgy. North Holland Physics Publ, Amsterdam, pp. 1595–1671.

Deer, W.A., Howie, R.A., Zussman, J., 1992. Rock Forming Minerals. Longmans, London 696pp.

Dornbusch, H.J., 1995. Gefüge-, Mikrostruktur- und Texturuntersuchungen an Hochtemperatur-Scherzonen in granulitfaziellen Metabasiten der Ivrea-Zone. Geotektonische Forschungen, 83, 94pp.

Dornbusch, H.J., Weber, K., Skrotzki, W., 1994. Development of microstructure and texture in high-temperature mylonites from the Ivrea Zone. In: Bunge, H.J., Siegesmund, S., Skrotzki, W., Weber, K. (Eds.). Textures of Geological Materials. Deutsch Gesellschaft für Materialkunde, Oberursel, pp. 187–201.

Drury, M.R., Urai, J.L., 1990. Deformation-related recrystallization processes. Tectonophysics 172, 235–253.

Drury, M.R., Humphreys, F.J., White, S.H., 1985. Large strain deformation studies using polycrystalline magnesium as a rock analogue. Part II: dynamic recrystallization mechanisms at high temperatures. Physics of the Earth and Planetary Interiors 40, 208–222.

Emmett, T.F., 1996. The provenance of pre-Scandian continental flakes within the Caledonide Orogen of south-cental Norway. In: Brewer, T.S. (Ed.). Precambrian Crustal Evolution in the North Atlantic Region. Geol. Soc. Special Publ. 112, pp. 359–366.

Escher, C., Gottstein, G., 1998. Nucleation of recrystallization in boron doped Ni_3Al. Acta Materialia 46, 525–539.

Etheridge, M.A., Hobbs, B.E., 1974. Chemical and deformational controls on recrystallization of mica. Contrib. Mineral. Petrol. 43, 111–124.

Fitz Gerald, J.D., Stünitz, H., 1993. Deformation of granitoids at low metamorphic grade. I: reaction and grain size reduction. Tectonphysics 221, 269–297.

Fitz Gerald, J.D., Etheridge, M.A., Vernon, R.H., 1983. Dynamic recrystallization in a naturally deformed albite. Textures and Microstructures 5, 219–237.

Fitz Gerald, J.D., Boland, J.N., McLaren, A.C., Ord, A., Hobbs, B.E., 1991. Microstructures in water-weakened single crystals of quartz. J. Geophys. Res. 96B, 2139–2155.

Fliervoet, T.F., 1995. Deformation mechanisms in fine grained quartzo–feldspathic mylonites — an electron microscpy study. Geologica Ultraiectina, 131, 167pp.

Fliervoet, T.F., White, S.T., 1995. Quartz deformation in a very fine grained quartzo–feldspathic mylonite: a lack of evidence for dominant grain-boundary sliding deformation. Journal of Stuctural Geology 17, 1095–1109.

Goode, A.D.T., 1978. High temperature, high strain rate deformation in the lower crustal Kalka intrusion, Central Australia. Contributions Mineralogy Petrology 66, 137–148.

Griffin, W.L., 1971. Genesis of coronas in anorthosites of the upper Jotun Nappe, Indre Sogn, Norway. Journal of Petrology 12, 219–243.

Griffin, W.L., Mellini, M., Oberti, R., Rossi, G., 1985. Evolution of coronas in Norwegian anorthosites: re-evaluation based on crystal-chemistry and microstructures. Contrib. Mineral. Petrol. 91, 330–339.

Hirsch, P., Howie, A., Nicholson, R., Pashley, D.W., Whelan, M.J., 1967. Electron Microscopy of Thin Crystals. Butterworths, London, 563pp.

Hirth, G., Tullis, J., 1992. Dislocation creep regimes in quartz aggregates. J. Struct. Geol. 14, 145–159.

Hossack, J.R., Garton, M.R., Nickelsen, R.P., 1985. The geological section from the foreland up to the Jotun thrust sheet in the Valdres area, south Norway. In: Gee, D.G., Sturt, B.A. (Eds.). The Caledonide Orogen — Scandinavia and Related Areas. John Wiley and Sons, New York, pp. 443–456.

Jensen, L.N., Starkey, J., 1985. Plagioclase microfabrics in a ductile shear zone from the Jotun Nappe, Norway. Journal of Structural Geology 7, 527–539.

Ji, S., Mainprice, D., 1988. Natural deformation of plagioclase: implication for slip systems and seismic anisotropy. Tectonophysics 147, 145–163.

Ji, S., Mainprice, D., 1990. Recrystallization and fabric development in plagioclase. Journal of Geology 98, 65–79.

Ji, S., Mainprice, D., Boudier, F., 1988. Sense of shear in high-temperature movement zones from the fabric asymmetry of plagioclase feldspars. Journal of Structural Geology 10, 73–81.

Karato, S., 1987. Seismic anisotropy due to lattice preferred orientation of minerals: kinematic or dynamic? In: Manghnani, M.H., Sono, Y. (Eds.). High Pressure Research in Mineral Physics. American Geophysical Union, pp. 455–471.

Karato, S., 1988. The role of recrystallization in the preferred orientation of olivine. Physics of the Earth and Planetary Interiors 51, 107–122.

Kruhl, J.H., 1987a. Computer assisted determination and representation of crystallographic orientations of plagioclase, on the basis of universal stage measurements. Neues Jahrbuch Mineralogie, Abhandlungen 157, 185–206.

Kruhl, J.H., 1987b. Zur Deformation und Gitterregelung des Plagioklases. Jahrbuch der Geologischen Bundesanstalt, Wien 130 (2), 205–243.

Kruse, R., 1998. Recrystallization and deforamtion mechanisms in mafic high temperature mylonites from the Jotun Nappe (S'Norway) and the Ivrea Zone (N'Italy). Ph.D thesis, Basel, 160pp.

Kruse, R., Stünitz, H., 1999. Deformation mechanisms and phase distribution in mafic high temperature mylonites from the Jotun Nappe, Southern Norway. Tectonophysics 303, 223–249.

Kunze, K., 1991. Zur quantitativen Texturanalyse von Gesteinen. Zentralinstitut für Physik der Erde. Ph.D thesis, Aachen, 136pp.

LaFrance, B., John, B.E., Scoates, J.S., 1996. Syn-emplacement recrystallization and deformation microstructures in the Poe Mountain anorthosite, Wyoming. Contributions Mineralogy Petrology 122, 431–440.

Lloyd, G.E., Farmer, A.B., Mainprice, D., 1997. Misorientation analysis and the formation and orientation of subgrain and grain boundaries. Tectonophysics 279, 55–78.

Mainprice, D., Lloyd, G.E., Casey, M., 1993. Individual orientation measurements in quartz polycrystals: advantages and limitations for texture and petrophysical property determinations. Journal of Structural Geology 15, 1169–1187.

Marshall, D.B., McLaren, A.C., 1977. Deformation mechanisms in experimentally deformed plagioclase feldspars. Physics and Chemistry of Minerals 1, 351–371.

McLaren, A.C., Pryer, L.L., 2001. Microstructural investigation of the interaction and interdependence of cataclastic and plastic mechanisms in feldspar crystals deformed in the semi-brittle field. Tectonophysics in press.

Milnes, A.G., Koestler, A.G., 1985. Geological structure of Jotunheimen, southern Norway (Sognefjell–Valdres cross-section). In: Gee, D.G., Sturt, B.A. (Eds.). The Caledonide Orogen — Scandinavia and Related Areas. John Wiley and Sons, New York, pp. 457–474.

Milnes, A.G., Wennberg, O.P., Skår, Ø., Koestler, A.G., 1997. Contraction, extension and timing in the South Norwegian Caledonides: the Sognefjord transect. In: Burg, J.P., Ford, M. (Eds.). Orogeny Through Time. Geol. Soc. London Spec. Publ. pp. 123–148.

Molli, G., 1994. Microstructural features of high temperature zones in gabbros of the Northern Apennine Ohiolites. Journal of Structural Geology 16, 1535–1541.

Olesen, N.Ø., 1987. Plagioclase fabric development in a high-grade shear zone, Jotunheimen, Norway. Tectonophysics 142, 291–308.

Olsen, T.S., Kohlstedt, D.L., 1984. Analysis of dislocations in some naturally deformed plagioclase feldspars. Physics of the Earth and Planetary Interiors 11, 153–160.

Olsen, T.S., Kohlstedt, D.L., 1985. Natural deformation and recrystallization of some intermediate plagioclase feldspars. Tectonophysics 111, 107–131.

Poirier, J.P., 1985. Creep of Crystals. Cambridge University Press, London, 260pp.

Poirier, J.P., Guillopé, M., 1979. Deformation induced recrystallization of minerals. Bulletin Minéralogie 102, 67–74.

Prior, D.J., 1999. Problems in determining misorientation axes, for small angular misorientations, using electron backscatter diffraction in the SEM. Journal of Microscopy 195, 217–225.

Randle, V., 1992. Microtexture Determination and its Applications. The Institute of Materials, London 174pp.

Randle, V., 1993. The Measurement of Grain Boundary Geometry. Institute of Physics Publishing, Bristol, 169pp.

Reinhard, M., 1931. Universal Drehtischmethoden. Webf and Cie, Basel, 119pp.

Schaeben, H., 1996. Texture approximation or texture modelling with components represented by the von Mises–Fisher matrix distribution on SO(3) and the Bingham Distribution on S^4_+. Journal of Applied Crystallography 29, 516–525.

Schärer, U., 1980. U–Pb and Rb–Sr dating of a polymetamorphic nappe terrain: the Caledonian Jotun Nappe, southern Norway. Earth and Planetary Science Letters 49, 205–218.

Schmid, S.M., 1982. Microfabric studies as indicators of deformation mechanisms and flow laws operative in mountain building. In: Hsü, K.J. (Ed.). Mountain Building Processes. Academic Press, London, pp. 95–110.

Schmid, S.M., 1994. Textures of geological materials: computer model predictions versus empirical interpretations based on rock deformation experiments and field studies. In: Bunge, H.J., Siegesmund, S., Skrotzki, W., Weber, K. (Eds.). Textures of Geological Materials. Deutsch Gesellschaft für Materialkunde, Oberursel, pp. 279–301.

Siegesmund, S., Helming, K., Kruse, R., 1994. Complete texture analysis of a deformed amphibolite: comparison between neutron diffraction and U-stage data. Journal of Structural Geology 16, 131–142.

Sondre Borges, F., White, S.H., 1980. Microstructural and chemical studies of sheared anorthosites, Roneval, South Harris. Journal of Structural Geology 2, 273–280.

Stünitz, H., 1998. Syndeformational recrystallization — dynamic or compositionally induced. Contribution to Mineralogy and Petrology 131, 219–236.

Toriumi, M., Karato, S., 1985. Preferred orientation development of dynamically recrystallized olivine during high temparature creep. Journal of Geology 93, 407–417.

Trépied, L., Doukhan, J.C., Paquet, J., 1980. Subgrain boundaries in quartz — theoretical analysis and microscopic observations. Physics and Chemistry of Minerals 5, 201–218.

Trimby, P.W., Prior, D.J., Wheeler, J., 1998. Grain boundary hierarchy development in a quartz mylonite. Journal of Structural Geology 20, 917–935.

Tullis, J., 1983. Deformation of feldspars. In: Ribbe, P.H. (Ed.). Feldspar Mineralogy. Am. Min. Soc., Washington, D.C., pp. 297–323.

Tullis, J., Yund, R.A., 1985. Dynamic recrystallization of feldspar: a mechanism for ductile shear zone formation. Geology 13, 238–241.

Tullis, J., Yund, R.A., 1987. Transition from cataclastic flow to dislocation creep of feldspar: Mechanisms and microstructures. Geology 15, 606–609.

Tullis, J., Yund, R.A., 1992. The brittle-ductile transition in feldspar aggregates: an experimental study. In: Evans, B., Wong, T.F. (Eds.). Fault Mechanics and Transport Properties of Rocks. Academic Press, London, pp. 89–117.

Tullis, J., Dell'Angelo, L., Yund, R.A., 1990. Ductile shear zones from brittle precursors in feldspathic rocks: The role of dynamic recrystallization. Geophys. Monograph 56, 67–81.

Turner, F.J., Weiss, L.E., 1963. Structural Analysis of Metamorphic Tectonites. McGraw-Hill, San Francisco, 545pp.

Urai, J.L., Means, W.D., Lister, G.S., 1986. Dynamic recrystallization of minerals. In: Hobbs, B.E., Heard, H.C. (Eds.). Mineral and Rock deformation: Laboratory studies. Geophysical monograph 36, 161–199, AGU, Washington, D.C.

Vernon, R.H., 1975. Deformation and recystallization of a plagioclase grain. American Mineralogist 60, 884–888.

Wenk, H.R., Bunge, H.J., Jansen, E., Pannetier, J., 1986. Preferred orientation of plagioclase — neutron diffraction and U-stage data. Tectonophysics 126, 271–284.

White, S., 1975. Tectonic deformation and recystallization of oligoclase. Contribution to Mineralogy and Petrology 50, 287–304.

Yund, R.A., Tullis, J., 1991. Compositional changes of minerals associated with dynamic recystallization. Contribution to Mineralogy and Petrology 108, 346–355.